AD-A071 446 UNIVERSITY OF SOUTHERN CALIFORNIA LOS ANGELES F/G 20/6
WAVEGUIDE STUDIES FOR FIBER OPTIC SOURCES.(U)
JUN 79 E GARMIRE F19628-77-C-0221
UNCLASSIFIED SCIENTIFIC-1 RADC-TR-79-112 NL

1 OF 1
ADA 071446

END
8-79

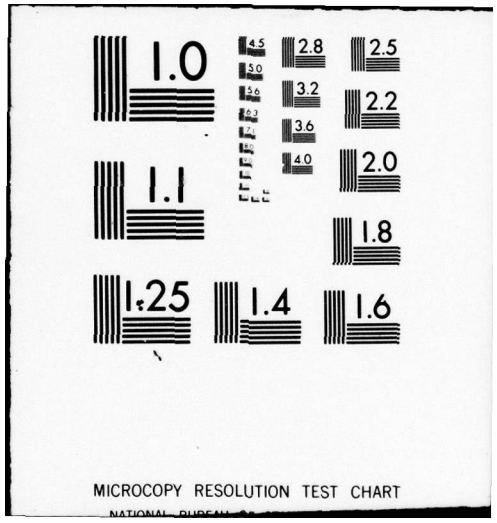
1.0
1.1
1.25
1.4
1.6
1.8
2.0
2.2
2.5
2.8
3.2
3.6
4.0
4.5
5.0
5.6
6.3
MICROCOPY RESOLUTION TEST CHART

RADC-TR-79-112
Interim Report
June 1979

WAVEGUIDE STUDIES FOR FIBER OPTIC SOURCES

University of Southern California

Elsa Garmire

LEVEL

ROME AIR DEVELOPMENT CENTER
Air Force Systems Command
Griffiss Air Force Base, New York 13441

This report has been reviewed by the RADC Information Office (OI) and is releasable to the National Technical Information Office (NTIS). At NTIS it will be releasable to the general public, including foreign nations.

RADC-TR-79-112 has been reviewed and is approved for publication.

APPROVED: Richard H. Picard

RICHARD H. PICARD
Contract Monitor

APPROVED: [signature]

ROBERT M. BARRETT, Director
Solid State Sciences Division

Accession For	
NTIS GRA&I	☒
DDC TAB	☐
Unannounced	☐
Justification	
By	
Distribution/	
Availability Codes	
Dist.	Avail and/or special
A	

FOR THE COMMANDER: John P. Huss

JOHN P. HUSS
Acting Chief, Plans Office

If your address has changed or if you wish to be removed from the RADC mailing list, or if the addressee is no longer employed by your organization, please notify RADC (ESO) Hanscom AFB MA 01731. This will assist us in maintaining a current mailing list.

Do not return this copy. Retain or destroy.

UNCLASSIFIED

SECURITY CLASSIFICATION OF THIS PAGE (When Data Entered)

REPORT DOCUMENTATION PAGE

READ INSTRUCTIONS BEFORE COMPLETING FORM

1. REPORT NUMBER: RADC-TR-79-112	2. GOVT ACCESSION NO.
3. RECIPIENT'S CATALOG NUMBER: Interim rept.	
4. TITLE (and Subtitle): WAVEGUIDE STUDIES FOR FIBER OPTIC SOURCES	5. TYPE OF REPORT & PERIOD COVERED: Scientific Report No. 1
	6. PERFORMING ORG. REPORT NUMBER: N/A
7. AUTHOR(s): Elsa Garmire	8. CONTRACT OR GRANT NUMBER(s): F19628-77-C-0221 new
9. PERFORMING ORGANIZATION NAME AND ADDRESS: University of Southern California, University Park, Los Angeles CA 90007	10. PROGRAM ELEMENT, PROJECT, TASK AREA & WORK UNIT NUMBERS: 61102F, 2306J228 — 17 J2
11. CONTROLLING OFFICE NAME AND ADDRESS: Deputy for Electronic Technology (RADC/ESO), Hanscom AFB MA 01731	12. REPORT DATE: June 1979
	13. NUMBER OF PAGES: 63
14. MONITORING AGENCY NAME & ADDRESS (if different from Controlling Office): Same — 12 68p.	15. SECURITY CLASS. (of this report): UNCLASSIFIED
	15a. DECLASSIFICATION/DOWNGRADING SCHEDULE: N/A

16. DISTRIBUTION STATEMENT (of this Report)

Approved for public release; distribution unlimited.

14 SCIENTIFIC-1

17. DISTRIBUTION STATEMENT (of the abstract entered in Block 20, if different from Report)

Same

18. SUPPLEMENTARY NOTES

RADC Project Engineer: Richard H. Picard (ESO)

Section V is reprinted from Optics Letters, Volume 3, by permission of the Optical Society of America. Copyrighted 1978.

19. KEY WORDS (Continue on reverse side if necessary and identify by block number)

Optical modulators	Semiconductor lasers
Electrooptic switches	Distributed Bragg gratings
Thin film waveguides	Bistable optical devices

79 07 19 019

20. ABSTRACT (Continue on reverse side if necessary and identify by block number)

Methods for multimode optical beam expansion, deflection, and switching are discussed in connection with fiber optic and optical signal processing applications. The feasibility of using negative waveguide lenses as beam expanders for stripe-geometry lasers is demonstrated. A monolithically integrated laser source and beam expander is designed utilizing planar epitaxy and selective chemical etches. Epilayer designs for optical coupling of light from the laser region to the waveguide are discussed. Grating distributed Bragg deflectors are fabricated, and the beam expansion from them is characterized. The use

next page

DD FORM 1 JAN 73 1473

361 550

UNCLASSIFIED

SECURITY CLASSIFICATION OF THIS PAGE (When Data Entered)

of electrical feedback to produce bistability in an optical switch in both bulk $LiNbO_3^2$ and $LiNbO_3^2$ waveguides is demonstrated, and the transient response of these hybrid bistable optical devices is investigated. Theoretical predictions of the dependence of switching time on applied ligh increment are confirmed.

TABLE OF CONTENTS

I. Introduction

Development of techniques for beam expansion is desirable to obtain a mode match between the output of a stripe geometry laser and a multimode fiber. In the proposal, it was suggested to produce waveguide beam expansion by a 45^{o} grating beam expander. The fabrication of such a device is underway. However, early experiments indicated that it is difficult to get short enough coupling lengths and high enough efficiencies to couple conveniently to optical fibers. It was, therefore, advantageous to look at other methods of expanding the beam. One of these is the negative waveguide lens. Calculations described in Section II, show that a negative waveguide lens can be designed with sufficient divergence to expand the beam from the narrow dimension of the stripe geometry laser to the wide dimension of the multi-mode optical fiber. It is therefore suggested that a monolithically integrated laser and negative waveguide lens can, in principle, be used to match the mode profile of the multimode optical fiber. This device is shown in Fig. I-1.

The beam expansion will take place on the same substrate as a monolithically integrated laser source. This requires developing designs for a monolithically integrated laser. In the proposal we suggested using non-planar epitaxy to develop the integrated optics

Figure I-1. Monolithic laser source including negative lens waveguide to expand the beam to fiber optics dimensions

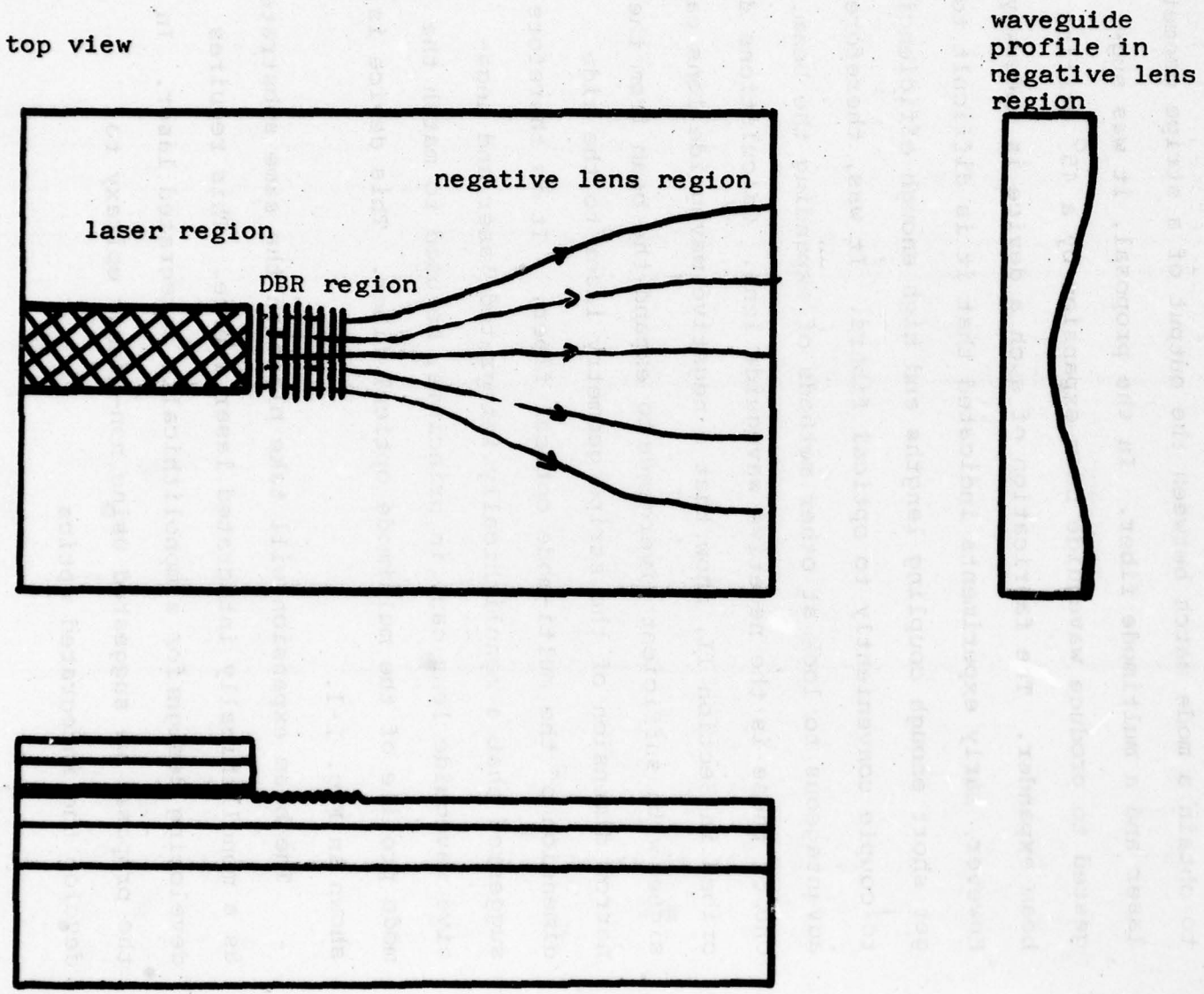

laser. As a result of this year's research, we have decided to use planar epitaxy and selective chemical etches. These techniques have been developed at Aerospace Corporation during the past year. In order to assure the feasibility of this technique, a study was made of the epilayer structure suitable for the most efficient operation. This requires an epilayer design in which light is coupled optimally from the laser waveguide to the passive waveguide. We have studied this problem and developed an epilayer design which is described in Section III and is summarized in Fig. I-2.

During the course of this contract, it was realized that the beam expander/deflector and other related concepts were applicable to the important problem of multimode switching for fiber optics applications and optical signal processing. This resulted in successful studies of the use of feedback in an optical switch producing bistability. This work is reported in a paper given at SPIE, Technical Symposium East, included as section IV, and also in a publication in Optics Letters, included as a reprint in section V. Recently we have made studies of the time-dependence of these switches, and a preprint of this research is included as section VI. It is intended that research continue in the second year on $LiNbO_3$ multimode switches for fiber optics applications.

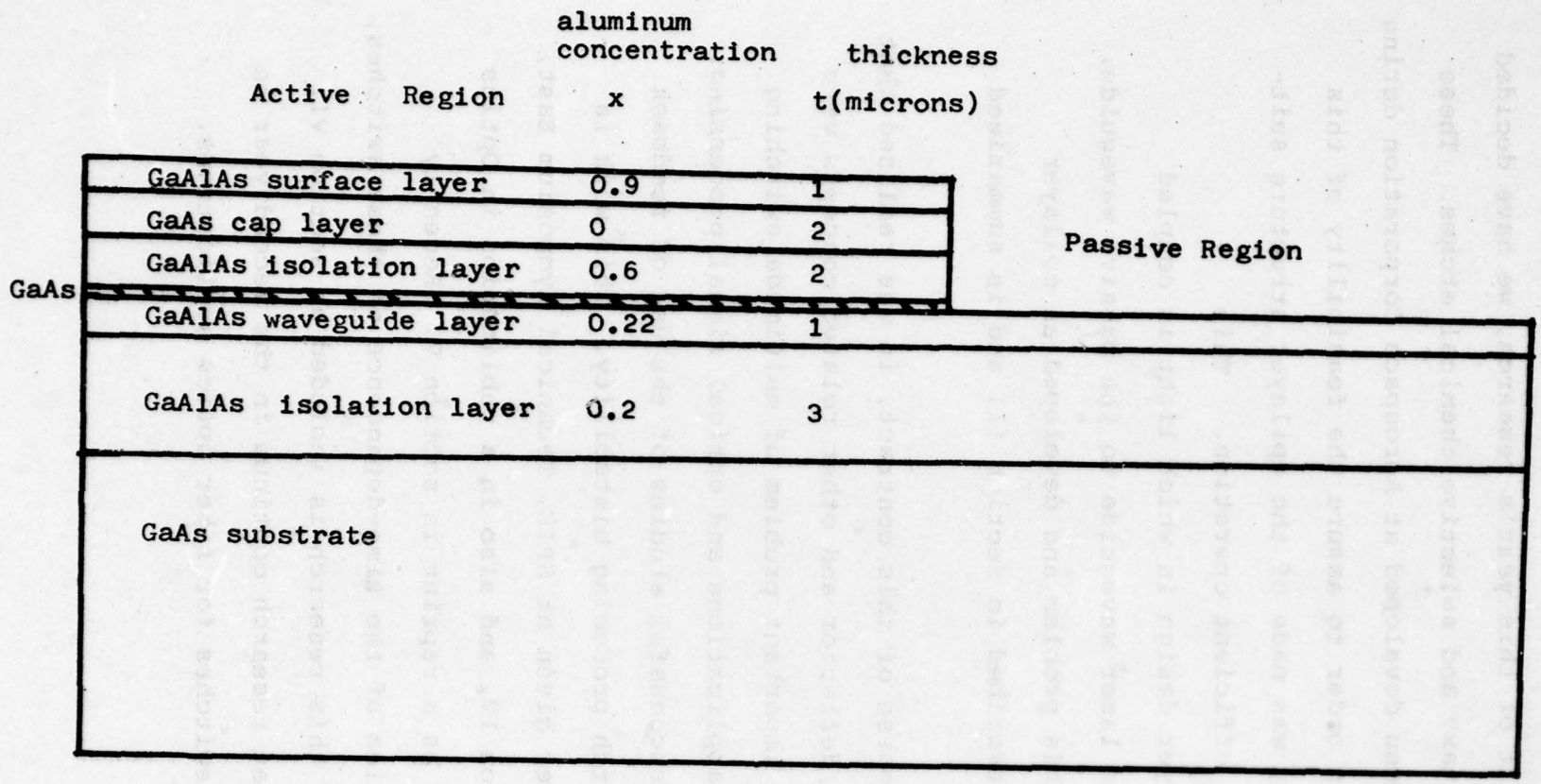

Figure 1-2. Optimized active/passive waveguide layer configuration

Initial efforts to fabricate and characterize the beam expansion of a 45° grating (Distributed Bragg Deflector or DBD) on GaAs were made at Aerospace Corporation on a subcontract. Deflection and resulting beam expansion were observed, but were limited by the inherent weakness of the process for waveguides with a low index discontinuity. The details are described in Section VII. Further measurements will be made in the coming year on GaAlAs waveguides in which the effect should be stronger.

II. Beam Expansion with Negative Waveguide Lenses

We have made a study of the possible use of a negative waveguide lens for beam expansion to match the single mode output of a stripe geometry laser to the dimensions of a multimode optical fiber. To this end, consider propagation of a Gaussian beam through a waveguide with a negative quadratic height profile.

Consider the quadratic waveguide profile shown in Fig. II-1. We shall show that this profile acts as a negative lens, expanding the beam.

We wish first to relate the properties of such a waveguide to those with a quadratic index variation. This can be done in an approximate way as long as the amount of curvature is small by using the V parameter of Marcuse to describe a waveguide. The propagation of a guide is characterized by $V=\sqrt{\Delta\epsilon}\ 2\pi t/\lambda$, where t is the waveguide thickness and $\Delta\epsilon$ is the dielectric discontinuity. It can be seen that changes in t cause a change in V the same as an equivalent change in the square root of the dielectric discontinuity. In particular, $\delta\Delta\epsilon/\Delta\epsilon=2\delta t/t$.

Let us consider a quadratic profile to the dielectric constant caused by a quadratic waveguide height profile.

$$\frac{\epsilon_{eff}}{\epsilon_{wg}} = 1 + \frac{2\,d\,r^2}{w_o^2}$$

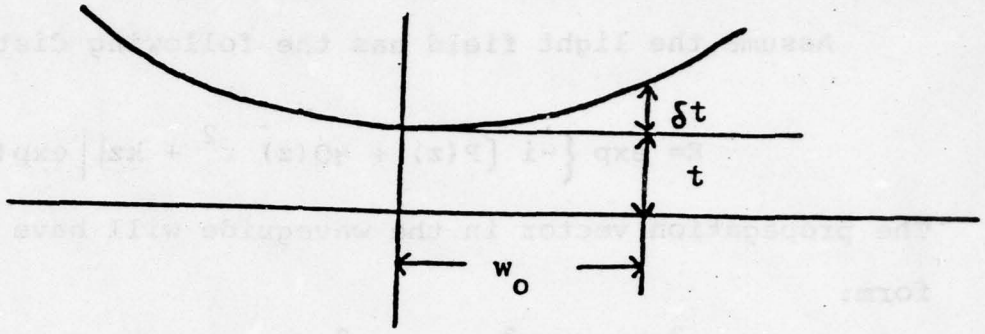

Figure II-1

Waveguide profile for negative lens

We have defined $d=\delta t/t$ at the beam radius, w_o. It is this positive quadratic change of effective dielectric constant which causes the beam expansion.

Assume the light field has the following distribution:

$$E= \exp\left\{-i\left[P(z) + \tfrac{1}{2}Q(z)\, r^2 + kz\right]\right\} \exp(+i\omega t)$$

The propagation vector in the waveguide will have the following form:

$$k^2(r) = k_o^2 - k_o k_2 r^2 \text{ where } k_o=\frac{2\pi}{\lambda_o} \text{ and } k_2=4\pi d\varepsilon/\lambda w_o^2.$$

Then the wave equation inside the waveguide becomes:

$$Q^2+k_oQ' -k_ok_2 = 0$$

$$P' = \frac{-iQ}{2k_o}$$

Now, define $q(z)=k_o/Q(z)$ then this quantity transforms by the following equation:

$$q(z) = \frac{Aq(0) + B}{Cq(0) + D}$$

where

$$A = \cosh \sqrt{\frac{k_2}{k_o}}\, z \qquad B=\sqrt{\frac{k_o}{k_2}} \sinh\sqrt{\frac{k_2}{k_o}}\, z$$

$$C = \frac{k_2}{k_o}\, B \qquad D = A$$

These are the same expressions as in Yariv (Intro. to Optical Electronics p. 39) if k_2 in his expression is made negative. Define $\sqrt{\frac{k_2}{k_o}} \equiv f$, and $q(0) = i\pi w_o^2/\lambda_0 \equiv iq_o$. Then we have

$$Q(z) = \frac{k_o}{q(z)} = k_o \frac{f^2Biq_o + A}{Aiq_o + B} = k_o f \left\{\frac{ifq_o \sinh fz + \cosh fz}{iq_o f\cosh fz + \sinh fz}\right\}$$

To obtain the beam waist at any point in this negative lens medium, we use the fact that $\frac{\lambda_o/\pi}{\mathrm{Im}\,Q(z)} = w^2(z)$. We therefore calculate

$$\mathrm{Im}\,Q(z) = \frac{-f^2 q_o}{(fq_o)^2\cosh^2 fz + \sinh^2 fz} .$$

This gives $w^2(z) = w_o^2 \left[(1 + fq)^{-2})\ \cosh^2 fz - (fq)^{-2}\right]$.

Writing $(fq)^{-2} = a = \{2\epsilon d\pi^2 (w_o/\lambda_o)^2\}^{-1}$ and $b = 2\epsilon\delta\ (w_o/\lambda_o)^{-1}$ we have

$$w^2 = w_o^2 \left[(1+a)\ \cosh^2\left(bz/\lambda_o\right) - a)\right] .$$

Consider numerically a specific case: $w_0 = 5\mu m$ (single mode GaAs laser)

$$w_o/\lambda_o = 6$$

$$\delta = 0.01$$

$$\epsilon = 3.5$$

then

$$a = 0.040$$

$$b = 0.044$$

This is shown in Fig. II-2. In addition, curves for different quadratic profiles are also included. It is to be observed that within a path length of 200 μm, beam expansion from a single mode laser stripe size (6 μm) to multimode fiber size (~100μm) is easily achievable. These data have questionable significance when $(w/w_o)^2 d \geq 1$, since the waveguide curvature is no longer a small perturbation. This limit is marked by the dotted line on the figure. In general this analysis is expected to be accurate for points below this line.

In summary, a negative waveguide lens appears theoretically to be a very reasonable way to achieve beam expansion from a single mode laser to a multimode fiber.

Figure II-2 Gaussian beam width in a negative lens waveguide as a function of path length

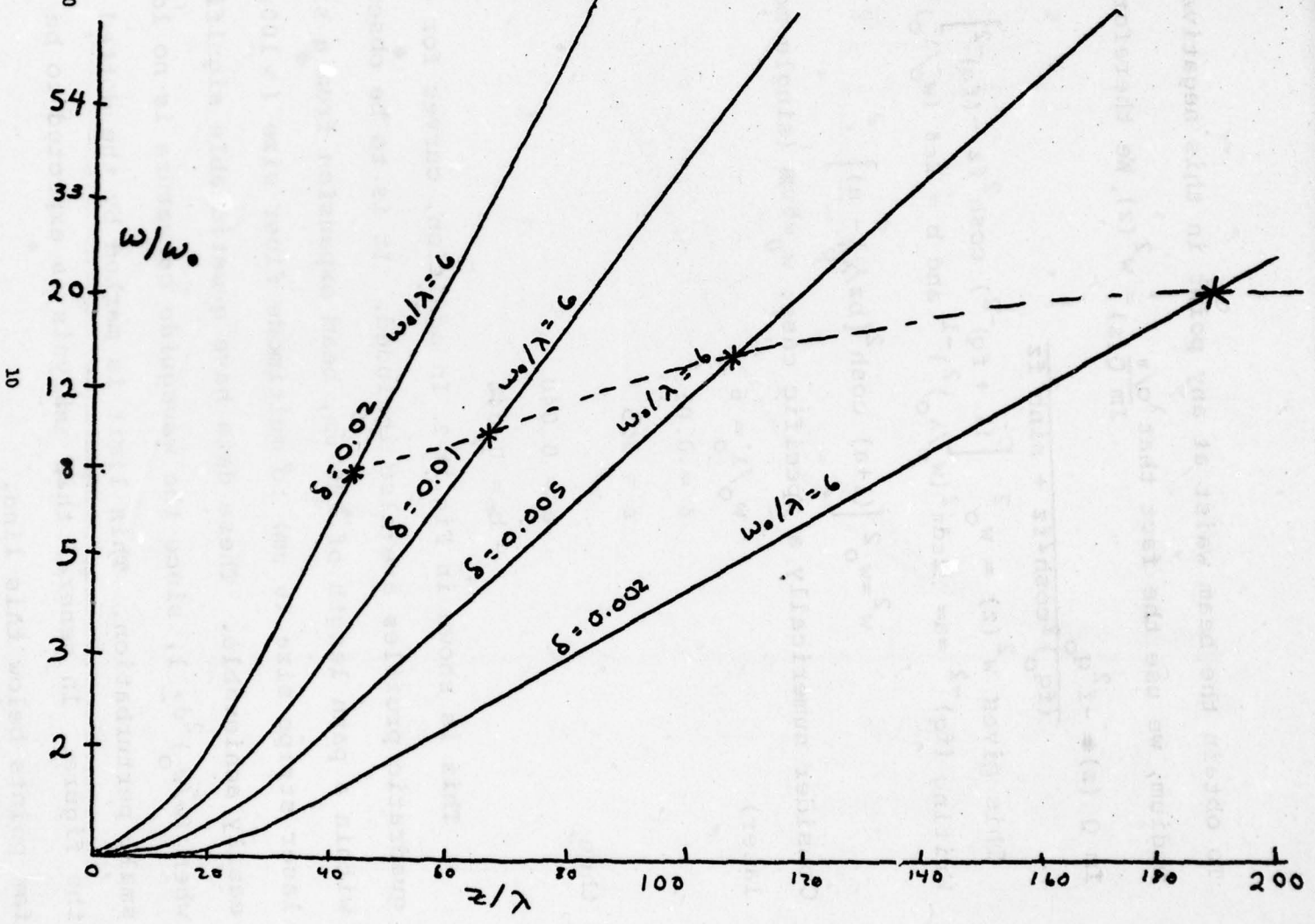

III. Integrated Optics Laser Epilayer Study

Referring to the design shown in Fig. I-2, the asymmetric AlAs concentration in the isolation layers surrounding the active region has several advantages. Most importantly, this allows the guided wave profile in the laser to match that in the passive waveguide region.

This can be seen by comparing Figs. III-1 and III-2. In Fig. III-1, the field profile in an air/guide/substrate configuration is compared with that in a symmetric embedded guide. In Fig. III-2 the field profile in an asymmetric guide is compared with that of the same waveguide with the top layer removed. It can be seen that the asymmetric structure has a better overlap.

Calculations have been made of the mode profiles for the four-layer asymmetric laser mode profile. A typical example is shown in Fig. III-3. The fourth layer is a thin localized gain region, included to confine the carriers and lower the threshold. We will show that this configuration has a high coupling efficiency and reasonably low threshold.

These modes were calculated in the usual waveguide fashion by matching boundary conditions. The dielectric discontinuity between layers 2 and 3 was chosen to give single mode propagation in the case of the passive waveguide. Since these layers are common between the laser and passive waveguide regions, they are determined by the requirements to ensure single mode propagation in the passive waveguide region. It turns out

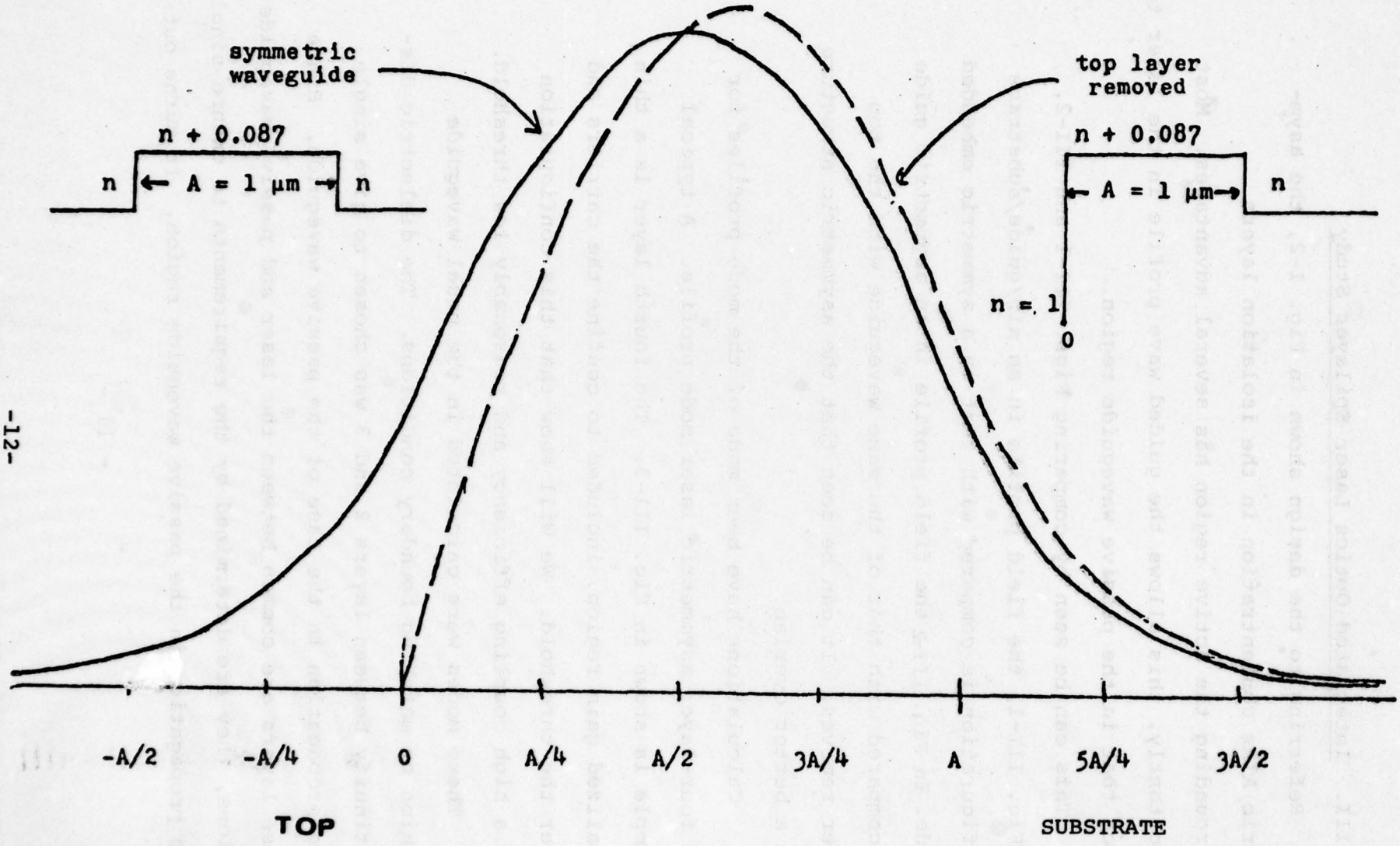

Figure III-1 TM mode field profiles for symmetric waveguide, and for same waveguide with the top layer removed.

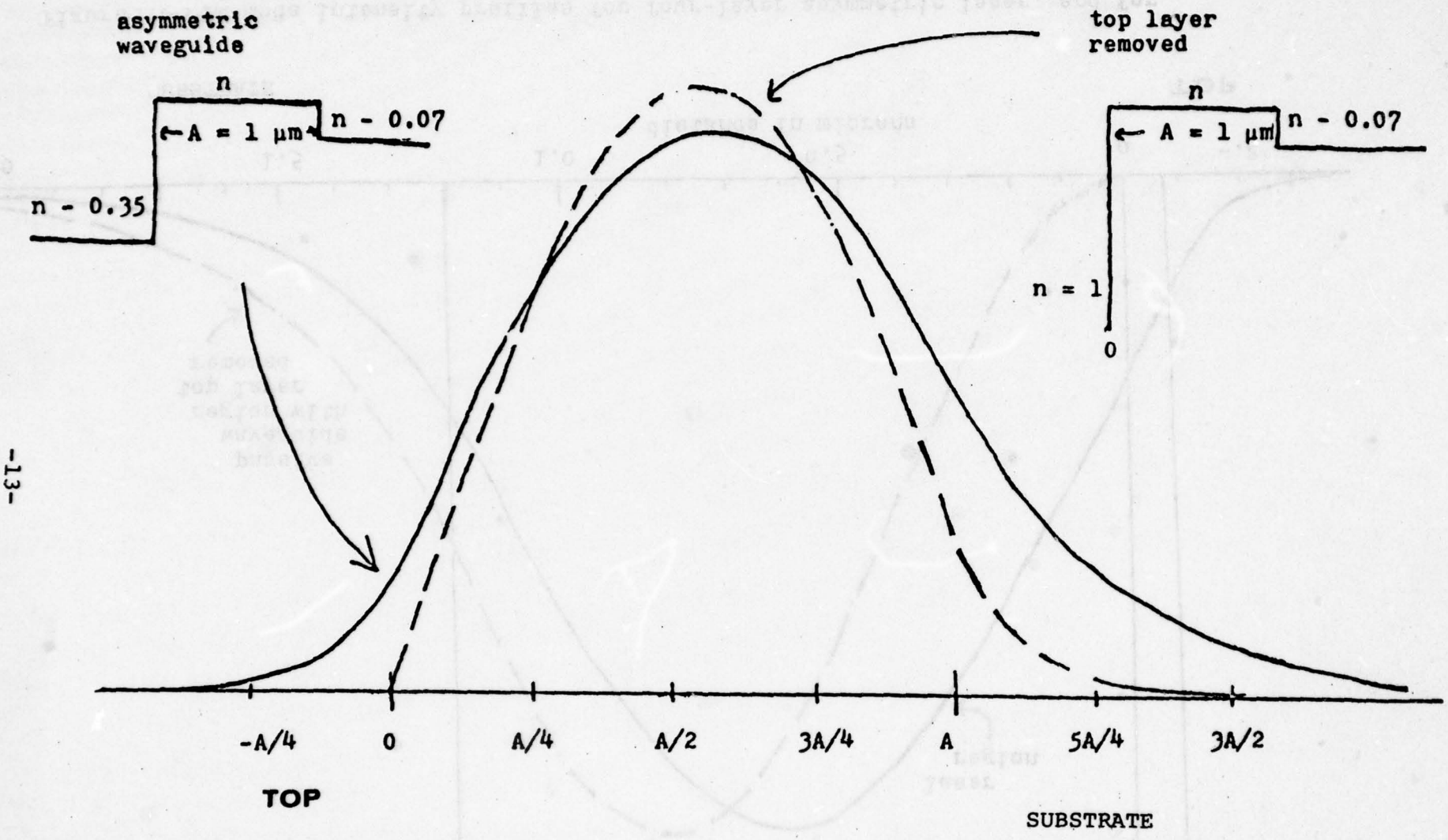

Figure III-2 TM mode field profiles for asymmetric waveguide, and for the same waveguide with the top layer removed

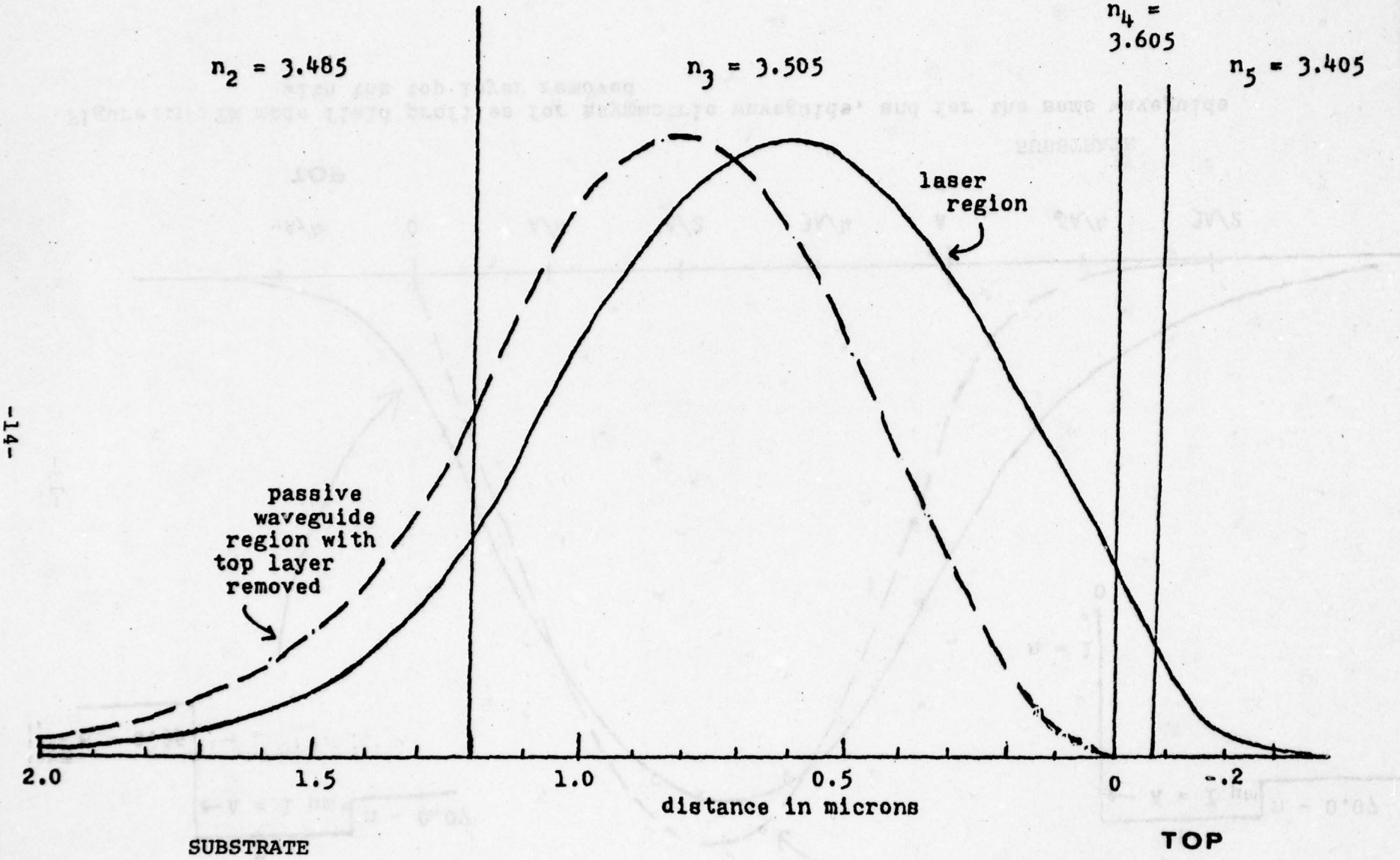

Figure III-3 TM mode intensity profiles for four-layer asymmetric laser, and for passive waveguide region with top layers removed

that this dielectric discontinuity enables more than one mode to propagate in the laser region, since its more symmetric structure has a less stringent waveguide cutoff condition. The presence of several modes in the laser region does not bother us, however, since only the lowest order mode couples efficiently into the single passive waveguide mode. This is therefore the only mode which will be above threshold in the DBR laser.

The best mode matching between the laser and passive waveguide regions would be a mode in which very little optical power is carried in the GaAs layer 4. This would make the threshold for these lasers very high, however. The optimum design, then, is a tradeoff between the possible increase in threshold and possible decrease in efficiency due to mode mismatch. Any meaningful analysis then requires calculation of laser threshold for any configuration of interest to determine if the threshold is within tolerable values. We have done this, following the analysis of Thompson[1], who gives an empirical equation for laser threshold which has been fit to experimental data of similar lasers. He finds that the fraction of light in the active region may be made rather small without increasing the threshold unduly if the active region is made very thin, since the increase in carrier density overcomes the decrease in optical density.

The thickness of the active region was specified at 0.07μm. This is the thinnest layer we have grown by LPE and was chosen as a representative target thickness. The waveguide modes were solved on a programmable calculator for varying values of Δn_5 and Δn_3. The aim of the calculations was to determine which

1. Thompson, Henshall, Whiteaway, and Kirkby, JAP 47 (4), 1501 (April 1976),

values of these dielectric discontinuities produced mode profiles which best matched those of the passive waveguide region, consistent with low laser threshold.

The laser threshold was calculated from the Thompson, et al. (eq. 3):

$$J_t = 4000B + 28B \left(\alpha - \frac{2}{L} \ln \left(\frac{n-1}{n+1}\right)\right) 1/f$$

where

B = thickness of active region in μm (region 4)
= .07 μm

α = absorption coefficient in cm^{-1}
= 10 cm^{-1}

f = fractional power in the active region

L = laser length = 0.05 cm.

Although this equation was fit to experimental 5 - layer LOC's the fifth layer was very thin (.1μm). Also, their theoretical analysis of the optical distribution used a 4-layer LOC, and this equation was determined to be valid.

Our calculations showed that the threshold decreased as the power in the active region increased. This occurred for decreasing n_3 or increasing n_5. As the power in the active region increased, the refractive index profile approached that of a symmetric waveguide, however, and the coupling efficiency decreased. The best design was therefore a trade-off between reduced coupling efficiency and increased threshold.

The aim of this design study was to maximize the coupling between the laser mode and the waveguide mode, consistent with low threshold. With both modes known, the coupling was calculated in the following way. The modes in the laser region, $E_L(x)$, were expanded in terms of the modes of the passive waveguide $E_W(x)$. Thus,

$$E_{Lj}(x) = \Sigma_i a_{ji} E_{Wi}(x)$$

These modes include both the waveguide modes and the continuum modes.

By orthogonality,

$$a_{ji} = \frac{\int E_{Lj} E_{Wi} \, dx}{\int E_W^2 \, dx}$$

The fraction of the laser power which is coupled into the passive waveguide modes is calculated differently for TE and TM modes, since the power is given by $\int E^2 dx$, the fraction of the laser power in mode j coupled into waveguide mode E_{Wi} is given by

$$f_{ij} = \frac{(\int E_{Wi} E_{Lj} \, dx)^2}{\int E_{Wi}^2 dx \int E_{Lj}^2 dx}$$

For TM modes, each region of the waveguide must be weighted by the inverse square of its refractive index. The power is given by: $(1/n^2)H^2 dx$, where n is considered to be n(x) and to have the appropriate value in each of the waveguide layers. Therefore, the fraction of TM power coupled from laser mode j into waveguide mode i is given by:

$$f_{ij} = \frac{\left(\int H_{Lj} H_{Wi}\, dx\right)^2 \int \frac{H_{wi}^2}{n^2}\, dx}{\left(\int H_{Wi}^2\, dx\right)^2 \int \frac{H_{Lj}^2}{n^2}\, dx}$$

After the mode profiles were determined, these integrals were evaluated on the calculator to determine the coupling coefficients. The results show that the design with parameters shown in Fig. III-3 has a TM threshold of 1.5 K amps/cm^2 with coupling efficiency of 88%. The TE threshold is 1.2 K amps/cm^2 with a coupling efficiency of 89%. It should be pointed out that these thresholds are for Fabry-Perot lasers and will be much the same for DBR lasers if proper grating reflectivities are chosen.

This calculation, coupled with the properties of selective chemical etches, has allowed us to design the layer structure shown in Fig. I-2.

To be published in Optical Engineering, 1979

IV. BISTABLE OPTICAL DEVICES FOR INTEGRATED OPTICS AND FIBER OPTICS APPLICATIONS

E. Garmire, S.D. Allen, J. Marburger

Center for Laser Studies
University of Southern California
University Park
Los Angeles, California 90007

ABSTRACT

A review of bistable optical devices is given, along with a description of a new class of devices which do not require Fabry-Perots.

INTRODUCTION

Electronically controlled optical switches are limited by capacitance and therefore have the speed of typical electronics. Faster switches are possible if optically controlled optical switches can be designed. Bistable optical devices are one particular class of such optically controlled optical switches. From the demonstration of bistability, we will show how that it is a straightforward extension to ultra-fast optically controlled optical circuits. In this paper we shall outline the concepts of optically controlled optical switches, and discuss their embodiment in nonlinear Fabry-Perots. We shall then discuss the use of hybrid electrical/optical switches and show results of experiments demonstrating optical bistability in a hybrid multimode integrated optics switch.

ALL-OPTICAL SWITCHES

Several advantages make all-optical switches very attractive. These are much the same advantages as have been identified for fiber optics. Ultra-fast switching is a key advantage and makes it possible to envisage switching which is not capacitance or electron transit-time limited. All-optical switches would have the same freedom from RFI and crosstalk as have optical fibers, and would also allow denser packing of optical switches than possible when electrical switching networks are used. In general, optical switching will utilize either three

or four port switches, as shown in Figure 1. The control either affects the transmission of a single channel in the three port case, or switches one channel between two output channels, in the four port case. The three port switch acts as an optical triode, with a weak control signal acting as the gate. When there is differential gain, a small control signal can be amplified at the output port, making an optical transistor. This has applications for optical repeaters and in situations where signal enhancement is required. Other applications are pulse shaping and optical limiting. The four port switch, in addition to providing a means of switching between two output channels, allows a number of logic functions to be performed, making possible optical signal processing and computation. If the two input channels are equivalent, the all-optical switch makes a high speed logic gate with many potential applications. An example of optical logic gates available from bistable optical devices are AND and OR. It will be seen that the bistable device has either a high transmission mode or a low transmission mode, depending on the input power level. By setting the appropriate discriminator level and combining the two input ports, the bistable device will switch from low to high transmission when either input signal is present, representing an OR. With a lower discriminator level, switching will take place only when both signals are present, representing an AND.

More complicated logic is available by combining these devices.

To produce an all-optical switch, one optical signal must affect the transmission of another. One way to do this is to use a device that has non-linear optical properties. We will show that a Fabry-Perot in a non-linear medium can make an optically controlled optical switch and exhibits bistability.(1) The non-linear Fabry-Perot is shown in Figure 2. With a good quality Fabry-Perot, the transmission is near 100% on resonance and otherwise near zero. Resonance is determined by requiring that the optical distance between mirrors is an integral number of wavelengths. That is, $M\lambda/(n_0 + n_2 I) = L$, where M is an integer and $n = n_0 + n_2 I$ is the non-linear refractive index and L is the length. When the Fabry-Perot is off-resonance, the light is reflected from the input face and the light level inside the Fabry-Perot is low. This is the low transmission mode of operation for the non-linear Fabry-Perot switch.

Consider a weak input signal, and a Fabry-Perot which is off-resonance, i.e.: in the low transmission mode. As the optical signal is increased, the non-linear refractive index increases until the Fabry-Perot goes into resonance. At this point, the device switches to the high transmission mode, and the transmitted field, (as well as the field inside the Fabry-Perot) suddenly increases. This behavior is shown in Figure 3 (increasing power direction). As the

intensity is slowly decreased, the transmission remains high, since the Fabry-Perot is high, and the cavity remains on resonance. Eventually, however, the non-linear phase shift is no longer sufficient to keep the Fabry-Perot on resonance, and the device suddenly switches to the off position. This is bistable operation with an optical hysteresis. (cf Fig. 3).

From the shape of Figure 3, the operation of the bistable device as an optical switch is apparent. Consider the input port as a holding signal with $I < I_{C1}$, while the control signal is superimposed on the holding signal. When the control signal $I_C > I_{C2} - I_{C1}$ the device switches. If the holding signal operates at an intensity $I_{C1} < I < I_{C2}$, the bistable device has a memory, keeping track of whether the last control signal was a bit (and switched the device to the high transmission mode) or a zero (keeping the device in the low transmission mode).

By tuning the Fabry-Perot, the distance between I_{C1} and I_{C2} may be reduced to zero, as shown in Figure 3b. In this configuration a weak control signal may cause a large change in output signal. This is the optical transistor with differential optical gain.

Non-linear Fabry-Perot's have been studied in experimental configurations utilizing sodium vapor (2) and ruby (3), as the non-linear cavity medium. Of greatest interest would be integrated optics version of such a device.

Here V_B is a bias voltage independent of P, and α is the conversion factor between detected optical power and voltage. This factor includes any necessary electronic amplification.

Writing $V_0 = \alpha P_0$, one may solve the implicit equation (2) for P or V by plotting the intersections of the straight lines V/V_0 with the transmission curve $T(V_B + V)$ vs. V, as described for a non-linear resonator device in reference (1). It is of course possible to solve explicitly for P_0 vs. P, but a construction which uses the familiar transmission curve T(V) has heuristic value. Whenever there are several intersections (values of V or P) for a given slope of the intersecting line (value of V_0 or P_0) then it is possible to construct a multistable optical device. The device will exhibit a hysteresis similar to that observed with the non-linear resonators discussed in previous work. (4) In fact, the hybrid Fabry-Perot devices are special cases of the broader class described here.

A particularly simple realization of this new class of devices is shown in Figure 5: This configuration is based upon the electro-optic polarization switch whose transmission in the ideal case is,

$$T(V) = \tfrac{1}{2} \{ 1 - F \cos (V + V_B + V_s) / V_h \} \qquad (3)$$

where V_h is the half-wave voltage, V_s is due to residual strain birefringence and F=1 in the presence of a perfect null. It is with this electro-optic polarization modulator that we have demonstrated bistability.

However, because of the inherent weakness of non-linear optical effects, such non-linear Fabry-Perot's require incident optical powers of the order MW/cm^2, which can be difficult to achieve in an IO format. In order to obtain bistable operation at lower power levels, it has been suggested (4) that an "artificial non-linearity" can be introduced by using the hybrid electrical/optical device shown in Figure 4. In this case the Fabry-Perot is filled with an electro-optic medium with transverse electrodes. A portion of the transmitted signal is detected, amplified and fed back across the electro-optic medium. This voltage controls the refractive index inside the Fabry-Perot and causes it to be on or off resonance in a fashion exactly analogous to the non-linear Fabry-Perot.

INCOHERENT MIRROR-LESS BISTABLE OPTICAL DEVICE

In a recent advance (5), we have demonstrated that a Fabry-Perot is not required to produce bistability in a hybrid electrical/optical device. In fact, a bistable switch can be constructed from any optical switch, whose transmission is a non-linear function $T(V)$ of an applied voltage V. The optical output power of such a switch is:

$$P = P_0 T(V) \qquad (1)$$

where P_0 is the input power. If the output is detected, and converted into a voltage, $V = \alpha P$, which is fed back to the switch, then the transmitted power obeys

$$P/P_0 = T(V_B + \alpha P). \qquad (2)$$

The modulator used in this experiment was a $LiNbO_3$ c-cut crystal 1x1 mm and 2 cm long with a half wave voltage of 260 V. This modulator was subject to voltage-dependent non-uniformities of the local electric field. As a result the transmission curve differed from the ideal form and is shown in Figure 6: The strain bias, V_s, was 60 V, and the null was 10% of the peak transmission value. The straight lines in Figure 5 correspond to the graphical solution of equation (2) described above for the critical input powers at which the device switches from one bistable state to the other.

Plots of light intensity out as a function of input light intensity are shown in Figure 7 for a number of bias voltages. These plots show the range of operating voltages over which hysteresis and bistability occurs. Hysteresis curves can be generated theoretically from the measured transmission curve by tracing the intersection of straight lines, whose slopes are the inverse of the intensity, with the transmission curve. Good agreement is obtained between the shape of the experimentally measured hysteresis curves and those derived from such a construction. From such construction, it can be seen that for this modulator bistability ceases for bias voltages $> -15V$, in agreement with measurements. Under optimum switching operation, the ratio of light transmitted in the on state to light trans-

mitted in the off state is ten to one. Furthermore, the hysteresis occurs over a large range of input intensities and bias voltages, making it easy to observe.

Bistable operation was dramatically evident in the following way. With a fixed laser intensity incident on the device, it could be switched from the low to the high transmission mode by shining a flashlight on the detector. The increase in laser transmission was quite obvious, and remained high indefinitely when the flashlight was turned off. When the incident intensity was interrupted, the transmission returned to its low value. This mode of operation is that of an optical triode, with the flashlight an incoherent control signal.

The experimental apparatus included a multimode 0.5 mW HeNe laser source, but a conventional light source could have been used as well. The modulator was an electro-optic polarization modulator, but could have been any device with non-linear transmission. The detector used to provide feedback tended to saturate when the intensity was a maximum. However, this non-linearity did not interfere with bistable operation; in fact, electronic non-linearities may be used to enhance bistability.

If the switch characteristic T (V) is known analytically, it is always possible to obtain an analytic expression for the bistable transfer wave (P_o V_s P)

$$P_o = P/T\ (V_B + P). \qquad (4)$$

The critical switching powers P_c are the values of P_o at the extrema of this curve, where

$$dP_o/dP = 0. \qquad (5)$$

For the ideal polarizer described by equation (3), this condition may be solved simultaneously with (4) to give

$$V_B = V_h \sin^{-1}(2V_h/FV_c) - \tfrac{1}{2}V_c \pm \tfrac{1}{2}(V_c^2F^2 - 4V_h^2)^{\frac{1}{2}} - V_s. \qquad (6)$$

This gives the relation between the critical field $V_C = \alpha P_C$ and the bias voltage V_B. (There are many pairs of bias voltages for each critical field and vice versa). Equations such as (6) allow accurate estimation of device operating parameters.

The elimination of resonators is an important advance when integrated optical multistable devices are considered, since it is difficult to obtain high Q's inside optical waveguides. With the knowledge that bistable operation may occur with any non-linear switch or modulator, given feedback from the transmitted signal, it is possible to contruct multistable modulators or devices using a variety of integrated optical switches such as directional couplers, polarization modulators, mode conversion or cutoff modulators, and beam deflectors. The operating powers and switching times of these devices will be similar to those of the hybrid Fabry-Perot device described by Smith and Turner. The integrated optics version of the incoherent bistable optical device appears to be well-suited for many optical processing applications.

INTEGRATED OPTICS BISTABLE MULTIMODE OPTICAL SWITCH

In order to demonstrate a multimode integrated optics version of the bistable device, we used an out-diffused $LiNbO_3$ y-cut waveguide 10 μm deep, with electrodes separated by 10 μm, to provide phase modulation for the TE mode. (6) This was converted to amplitude modulation by interference with unmodulated light. The transmission of this modulator as a function of voltage is shown in Figure 8. Because of non-uniformities in the incident light and in the applied field, the transmission was not a periodic function of the voltage. This fact is useful in demonstrating the principle that bistability does not require periodic optical switches. The bistable region lies between the straight lines in Figure 8, which correspond to the graphical solutions of Equation 1, described above, for the critical input powers at which the device ceases to be bistable.

Plots of light intensity out as a function of input light intensity are shown in Figure 9 for several bias voltages and are seen to have sharper switching characteristics than the bulk device.

These two experiments demonstrate that integrated optics BOD's can be made very simply and compactly. The concepts presented here show that any voltage-controlled modulator, switch or beam deflector may be made bistable. As a result, it is possible to design integrated optics BOD's optimized for specific applications. This includes

polarization-insensitive, incoherent or multimode devices as well as compact single mode devices. This result has important implications concerning the ultimate usefulness and versatility of these devices.

REFERENCES

1. F.S. Felber, J.H. Marburger, Appl. Phys. Lett. 28, 731 (1976). J.H. Marburger, and F.S. Felber, Phys. Rev. A. 17, 335 (1978).

2. H.M. Gibbs, S.L. McCall, T.N.C. Vankatesan, Phys. Rev. Lett. 36, 1135 (1976).

3. T.N.C. Vankatesan, S.L. McCall, Appl. Phys. Lett. 30, 282 (1977).

4. P.W. Smith and E.H. Turner, Appl. Phys. Lett. 30, 280 (1977).

5. E. Garmire, J. Marburger, S.D. Allen, Appl. Phys. Lett. 31, 320 (1978).

6. E. Garmire, S.D. Allen, J. Marburger, C.M. Verber, Optics Letters, 3, 69 (1978)

FIGURE CAPTIONS

IV-1a) Three port optical switch

IV-1b) Four port optical switch

IV-2) Non-linear Fabry-Perot

IV-3) Output light intensity of a non-linear Fabry-Perot as a function of input light intensity for two differently tuned cavities. The arrows show the path taken by the device when a slowly varying input pulse is applied.

IV-4) Hybrid electrical/optical Non-linear Fabry-Perot

IV-5) Experimental apparatus for the incoherent mirrorless bistable optical device using an electro-optic polarization modulator.

IV-6) Transmission is a function of voltage for the electro-optic modulator through crossed polarizer and analyzer. Straight lines represent the limits of bistable operation for $V_B = -120$ V.

IV-7) Light out of the bistable device as a function of the light in, for a number of bias voltages, demonstrating hysteresis characteristic of bistable operation.

IV-8) Transmission of waveguide switch as a function of applied voltage.

IV-9) Output intensity vs. input intensity with bistable waveguide switch for different bias voltages.

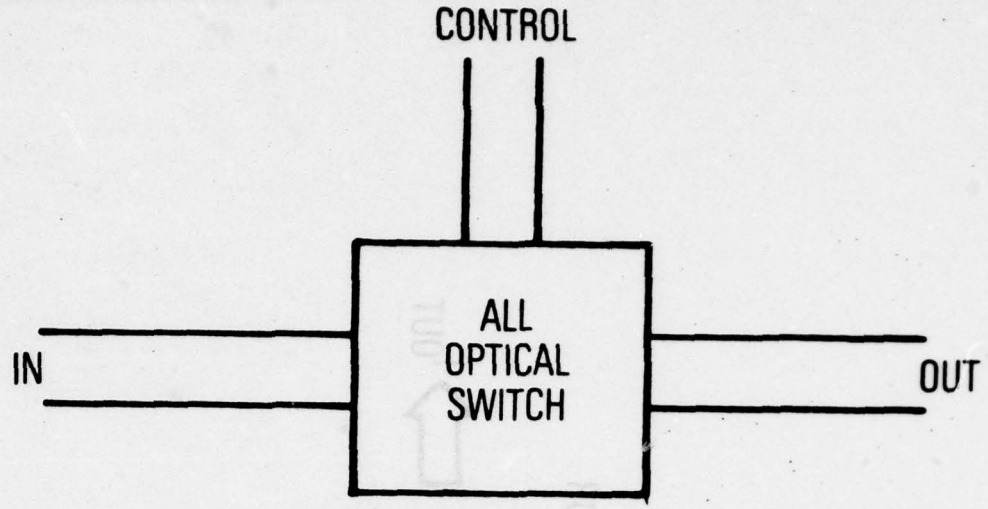

Figure IV-1a. Three port optical switch

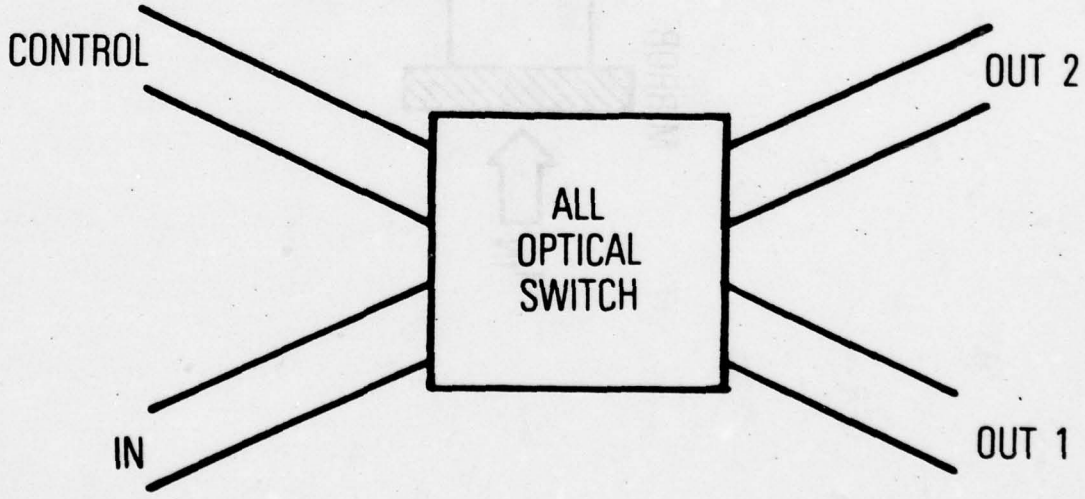

Figure IV-1b. Four port optical switch

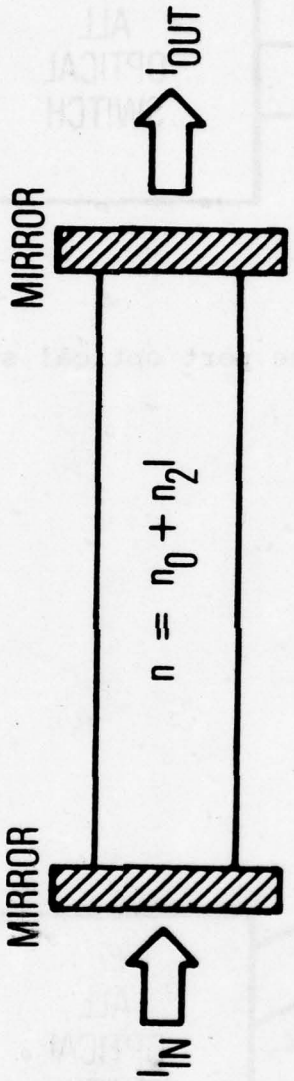

Figure IV-2. Non-linear Fabry-Perot

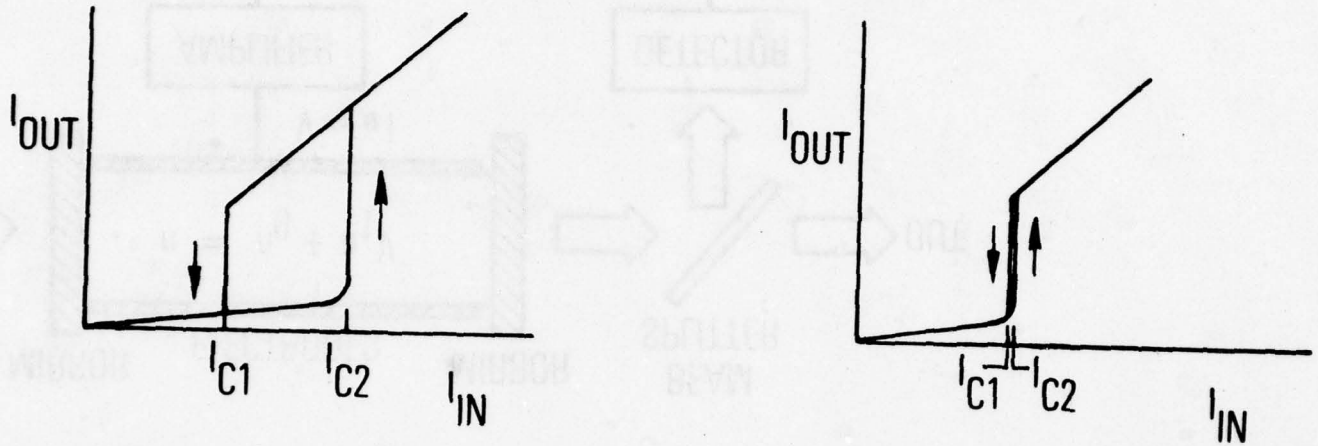

Figure IV-3. Output light intensity of a non-linear Fabry-Perot as a function of input light intensity for two differently tuned cavities. The arrows show the path taken by the device when a slowly varying input pulse is applied.

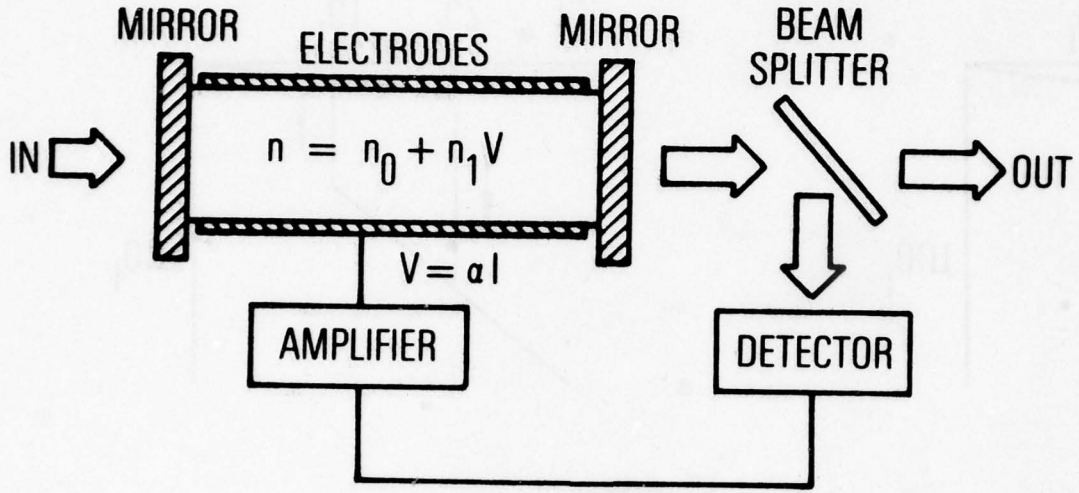

Figure IV-4. Hybrid electrical/optical Non-linear Fabry-Perot

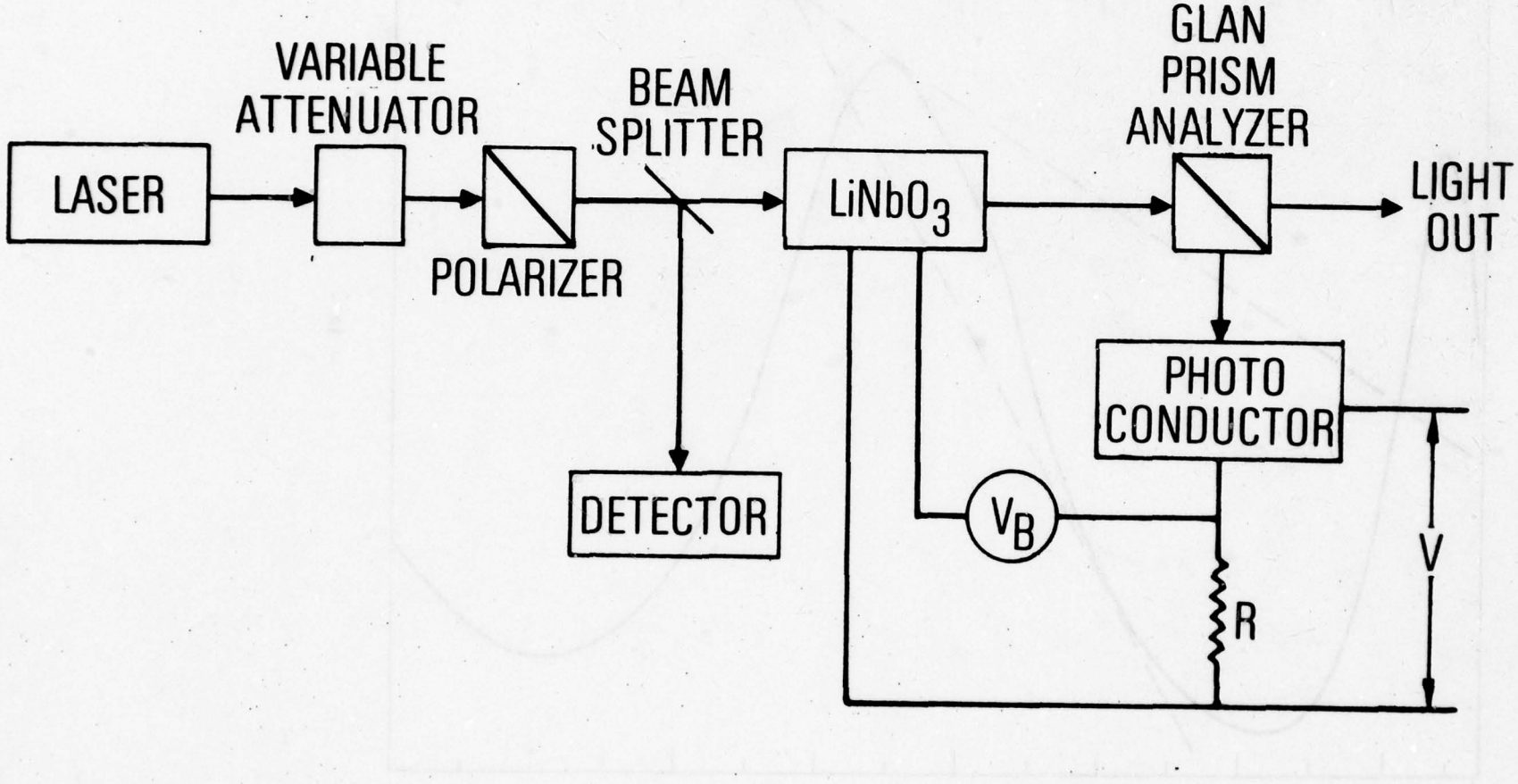

Figure IV-5. Experimental apparatus for the incoherent mirrorless bistable optical device using an electro-optic polarization modulator.

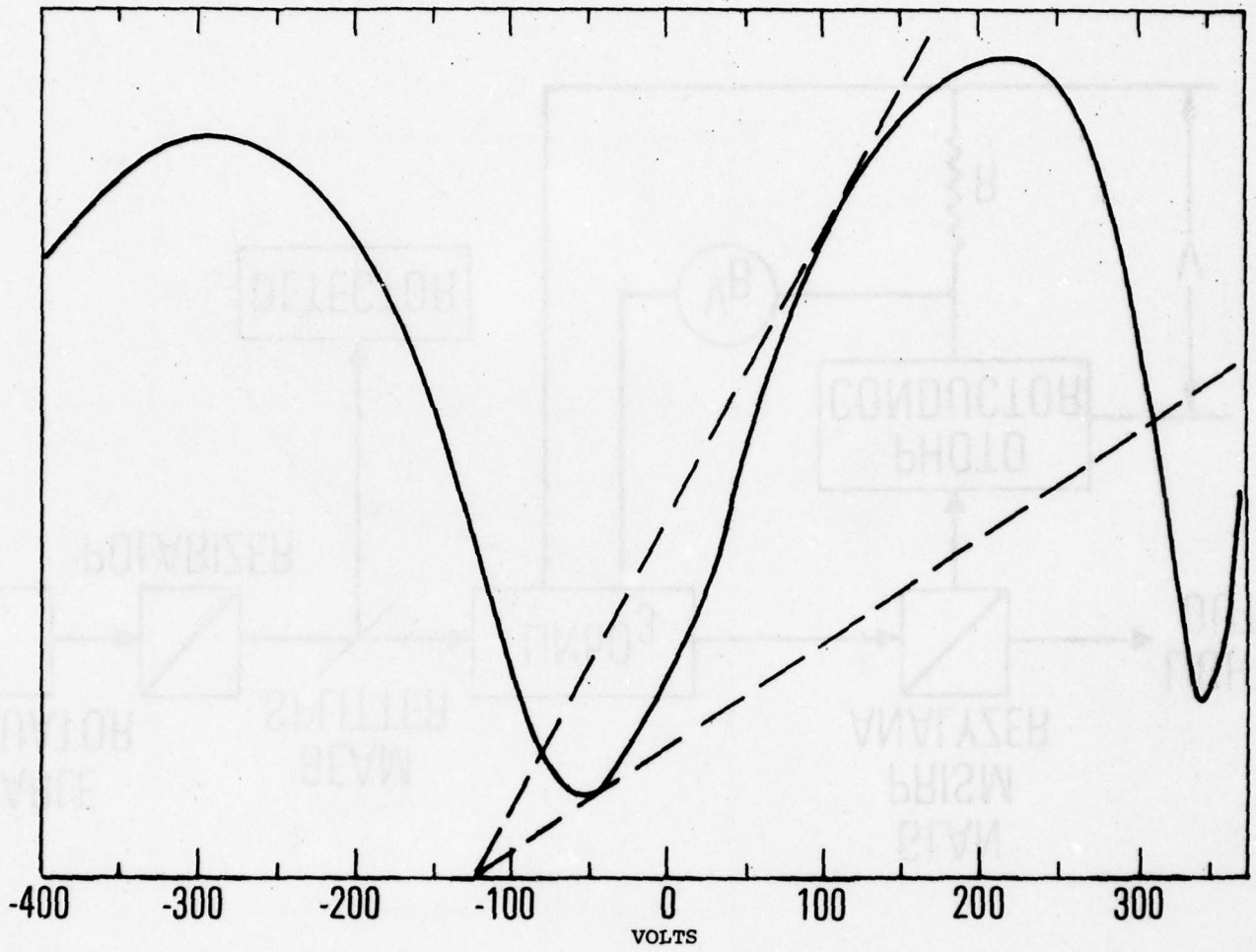

Figure IV-6. Transmission is a function of voltage for the electro-optic modulator through crossed polarizer and analyzer. Straight lines represent the limits of bistable operation for V_B = 120 V.

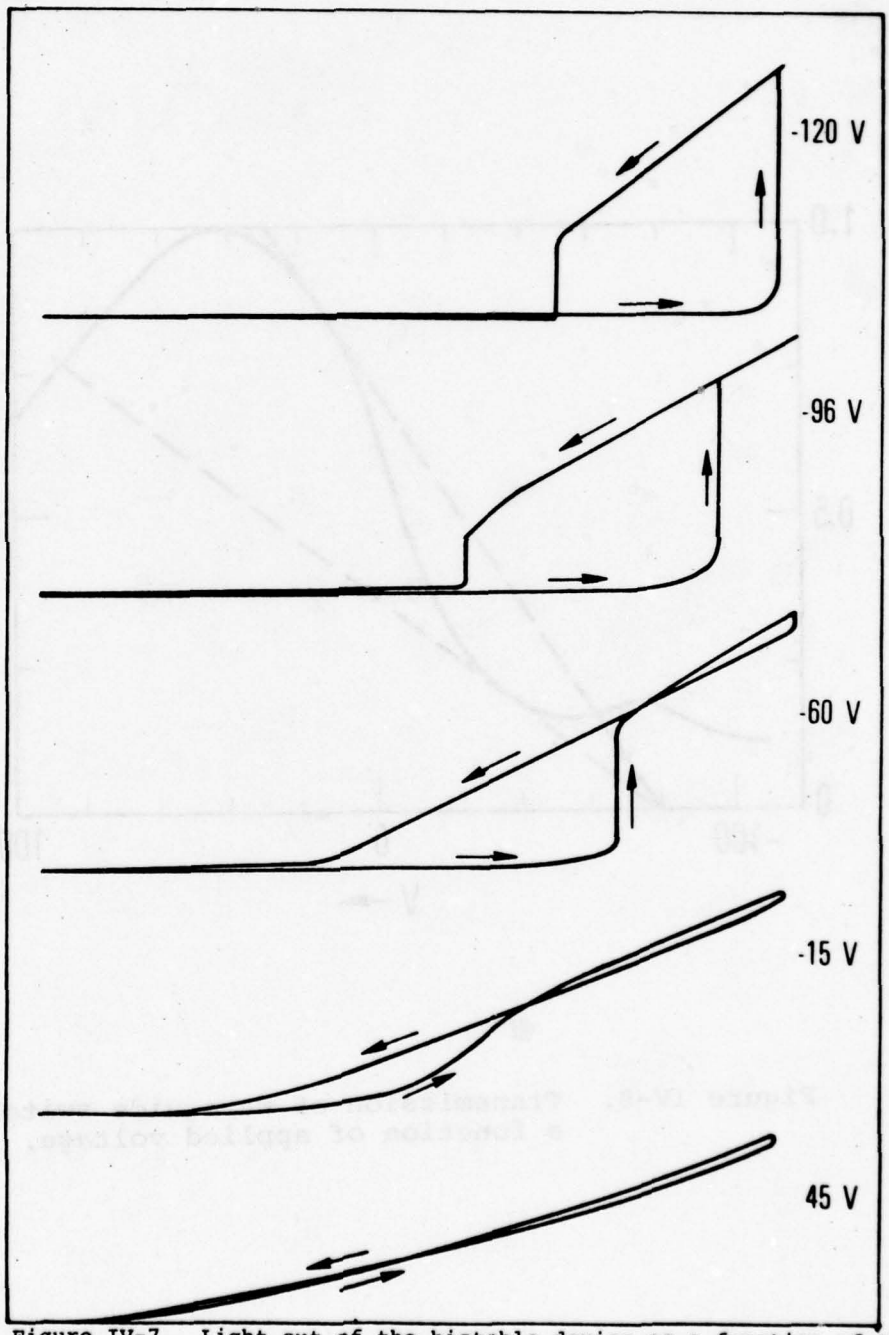

Figure IV-7. Light out of the bistable device as a function of the light in, for a number of bias voltages, demonstrating hysteresis characteristic of bistable operation.

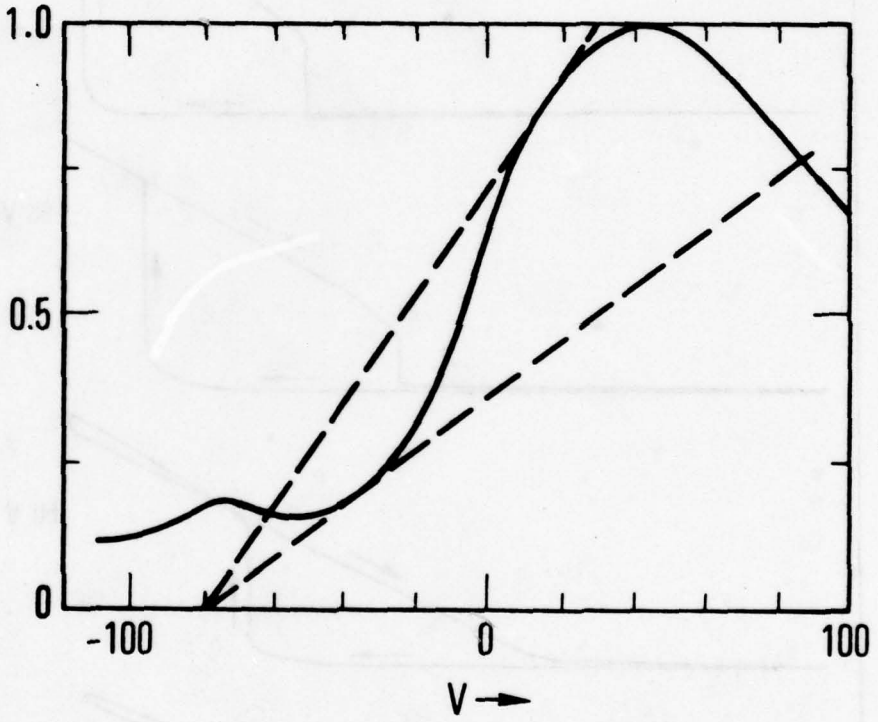

Figure IV-8. Transmission of waveguide switch as a function of applied voltage.

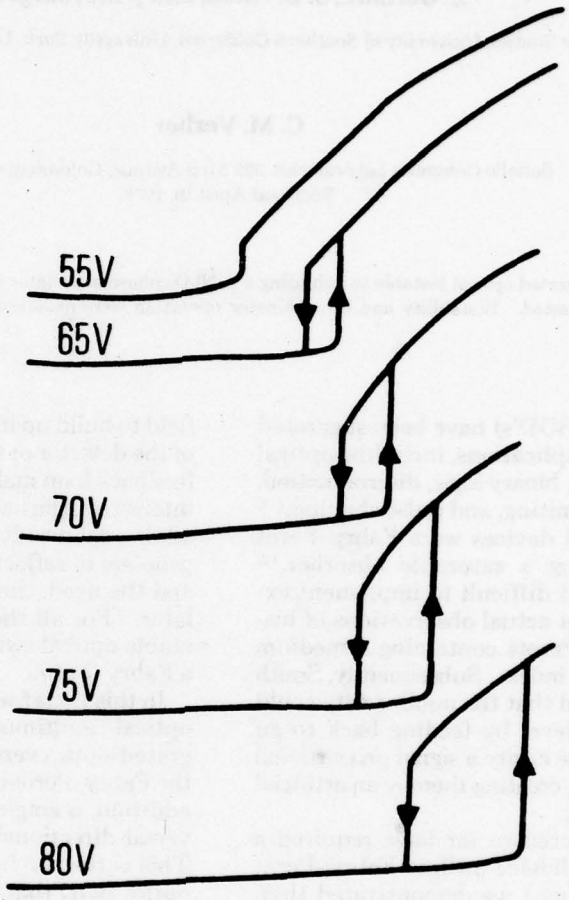

Figure IV-9. Output intensity vs. input intensity with bistable waveguide switch for different bias voltages.

Reprinted from OPTICS LETTERS, Vol. 3, page 69, August 1978

V. Multimode integrated optical bistable switch

E. Garmire, S. D. Allen, and J. Marburger

Center for Laser Studies, University of Southern California, University Park, Los Angeles, California 90007

C. M. Verber

Battelle Columbus Laboratories, 505 King Avenue, Columbus, Ohio 43201
Received April 10, 1978

A multimode integrated optical bistable switch using a $LiNbO_3$ phase modulator in a noncavity configuration was constructed and tested. Bistability and discriminator operation were observed in this device using a He–Ne laser.

Bistable optical devices (BOD's) have been suggested for many optical device applications, including optical switching, optical memory, binary logic, discrimination, amplification, clipping, limiting, and pulse shaping.[1-6] The first bistable optical devices were Fabry–Perot interferometers containing a saturable absorber.[1,2] This configuration proved difficult to implement experimentally, and the first actual observations of bistability[3] were in Fabry–Perots containing a medium with a nonlinear refractive index. Subsequently, Smith and Turner[5] demonstrated that the nonlinearity could be induced at low light level by feeding back to an electro-optic element in the cavity a signal proportional to the output of the cavity, creating thereby an artificial nonlinear refractive index.

All the devices considered so far have required a single-mode laser, since all have utilized Fabry–Perot cavities. In a recent paper,[7] we demonstrated that, when electrical feedback is employed, the Fabry–Perot cavity is not required. It is therefore possible to make bistable optical devices from any optical element with a nonlinear transmission as a function of applied voltage by feeding back an electrical signal proportional to the detected intensity. These devices obey the following equation for the transmitted power:

$$P = P_0 T(V_B + \alpha P), \tag{1}$$

where P and P_0 are transmitted and incident intensity, respectively, $T(V)$ is the transmission function, V_B is a bias voltage independent of P, and α is the feedback proportionality constant. A macroscopic $LiNbO_3$ polarization modulator with feedback from the detector to the modulator electrodes served as the experimental verification of the broad range of devices that fall into this category.

We have demonstrated that all BOD's require some sort of feedback; this may be optical or electrical, but it need not be both. When electrical feedback is available, the use of a Fabry–Perot is not required. Although the resonance of the Fabry–Perot decreases the optical power required to switch the device, the switching time is increased by the time required for the field to build up inside the cavity. Since the sensitivity of the detector or the use of an amplifier in the electrical feedback loop makes possible switching at low incident intensities, the need for a Fabry–Perot is obviated. An additional disadvantage of using a Fabry–Perot is the problem of reflected light coupling back into the laser and the need, therefore, to incorporate an optical isolator. For all these reasons, using the mirrorless bistable optical switch has many advantages over using a Fabry–Perot.

In this Letter we extend this concept to an integrated optical multimode bistable optical device. Integrated-optics versions of bistable optical devices using the Fabry–Perot configuration have been reported.[8] In addition, a single-mode mirrorless device using β reversal-directional coupler switch has been reported.[9] This is the the first report of a multimode integrated optics BOD that will have applications in fiber optics and other multimode systems. This hybrid electrical–optical device uses electrical feedback from a detector to a multimode electro-optical waveguide modulator to achieve bistability. The device will be described and performance data presented.

The 10-μm-deep waveguide was formed by out-diffusion in y-cut $LiNbO_3$, and electrodes separated by 10 μm provided phase modulation for the TE mode. Interference with unmodulated light converted the phase modulation into amplitude modulation. The experi-

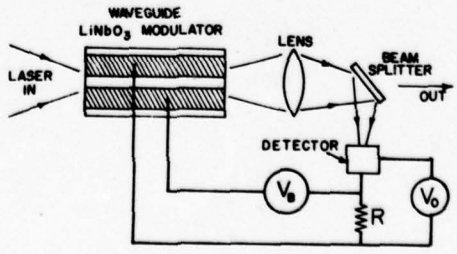

Fig. 1. Integrated-optics mirrorless bistable optical device using a waveguide $LiNbO_3$ phase modulator with an active length of 2 mm.

0146-9592/78/0800-0069$0.50/0

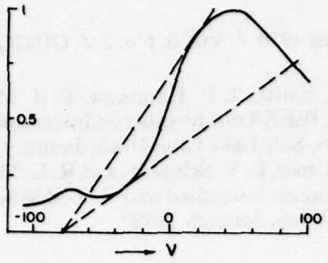

Fig. 2. Transmission of $LiNbO_3$ modulator as a function of applied voltage. Vertical scale in arbitrary units.

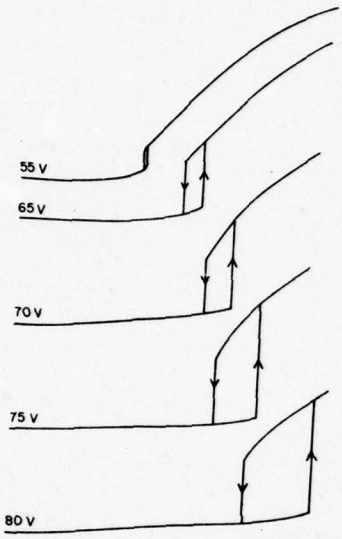

Fig. 3. Output intensity versus input intensity for different bias voltages.

mental setup is shown in Fig. 1. A 0.5-mW He–Ne laser was coupled into the waveguide with a microscope objective and the output beam refocused on an aperture in front of the detector. The transmission of the modulator as a function of applied voltage is shown in Fig. 2. The length of the modulator was only 2 mm; hence the relatively large voltages.

Because of nonuniformities in the incident light and in the applied field, the transmission was not a periodic function of the voltage. This fact is useful in demonstrating the principle that bistability does not require periodic optical switches. The bistable region lies between the straight lines in Fig. 2, which correspond to the graphical solutions[7] of Eq. (1), for the critical input powers at which the device ceases to be bistable. A periodic switch would have been multistable, with a bistable region associated with each peak of the transmission curve.

Plots of output light intensity as a function of input light intensity for several bias voltages are shown in Fig. 3. These plots show the range of operating voltages over which hysteresis and bistability occur. Hysteresis curves can be generated theoretically from the measured transmission curve by the graphical method described in Ref. 7. Good agreement is obtained between the shape of experimentally measured hysteresis curves and those derived from such a construction. Under optimum switching operation, the ratio of light transmitted in the on state to light transmitted in the off state is greater than ten to one. Furthermore, the hysteresis occurs over a large range of input intensities and bias voltages, making it easy to observe.

It is of interest to compare these hysteresis curves with those of the bulk modulator previously published[7] and to notice that the integrated-optics version has much sharper switching action. The lack of sharp cutoff switching in the bulk device was due in part to the particular shape of the transmission function and in part to a long time constant arising from the large capacitance of the bulk device.

The integrated-optics version demonstrates a region of differential amplification or optical-transistor action when the critical on and off voltages slightly merge (55-V bias, as seen in Fig. 3). At bias voltages slightly larger than this, the integrated-optics BOD makes an excellent discriminator.

The integrated-optics modulator was only 2 mm long. This is an order of magnitude smaller than the bulk modulator. Such a waveguide bistable switch can be made as small as desired, limited only by the voltage that can be applied. On the other hand, much lower switching voltages may be used with long modulators.

A fully integrated version of the multimode bistable optical switch would include a detector integrated onto the modulator. A device fabricated in this fashion would have switching times even faster than those quoted by Smith and Turner,[5,6] since there is no time needed for the field to build up in a Fabry–Perot resonator.

The integrated-optics bistable switch we report here is a three-port switch. However, a multimode four-port switch can be built using a polarization modulator and an integrated-optics analyzer.

The data and concepts presented here show the feasibility of multimode-waveguide bistable optical devices. In fact, any modulator, switch, or beam deflector can be made bistable with appropriate feedback. The device described herein was certainly not optimized for this experiment, but bistability was easily observed. As a result, it should be possible to design integrated-optics BOD's for specific applications. This includes polarization-insensitive, incoherent, or multimode devices as well as compact single-mode devices. This result has important implications concerning the ultimate usefulness and versatility of these devices.

This research was sponsored by RADC/ETSO, Hanscom Air Force Base, Massachusetts.

References

1. H. Seidel, U.S. Patent 3,610,731 (1969).
2. A. Szöke, V. Daneu, J. Golhar, and N. A. Kurnit, Appl. Phys. Lett. **15**, 376 (1969).
3. H. M. Gibbs, S. L. McCall and T. N. C. Venkatesan, Phys. Rev. Lett. **36**, 1135 (1976); T. N. C. Venkatesan and S. L. McCall, Appl. Phys. Lett. **30**, 282 (1977).
4. F. S. Felber and J. H. Marburger, Appl. Phys. Lett. **28**, 731 (1976); J. H. Marburger and F. S. Felber, Phys. Rev. A **17**, 335 (1978).

5. P. W. Smith and E. H. Turner, Appl. Phys. Lett. **30**, 280 (1977).
6. P. W. Smith, E. H. Turner, and P. J. Maloney, IEEE J. Quantum Electron. **QE-14**, 207 (1978).
7. E. Garmire, J. H. Marburger, and S. D. Allen, Appl. Phys. Lett. **32**, 320 (1978).
8. P. W. Smith, I. P. Kaminow, P. J. Maloney, and L. W. Stutz, IEEE/OSA Meeting on Integrated and Guided Wave Optics, Salt Lake City, Utah, January 1978.
9. P. S. Cross, R. V. Schmidt, and R. L. Thanton, IEEE/OSA Meeting on Integrated and Guided Wave Optics, Salt Lake City, Utah, January 1978.

To be published in Applied Physics Letters, March, 1979.

TRANSIENT RESPONSE OF HYBRID BISTABLE OPTICAL DEVICES

E. Garmire, J.H. Marburger, S.D. Allen, and H.G. Winful

Center for Laser Studies
University of Southern California
University Park
Los Angeles, California 90007

ABSTRACT

The response of a hybrid bistable optical device to step inputs of light was studied experimentally. The results confirm theoretical predictions concerning the dependence of switching time on the applied light increment. For the first time the phenomenon of "critical slowing down" is observed directly.

TRANSIENT RESPONSE OF HYBRID BISTABLE OPTICAL DEVICES

E. Garmire, J.H. Marburger, S.D. Allen and H.G. Winful

Center for Laser Studies
University of Southern California, University Park
Los Angeles, California 90007

Bistable optical devices (BOD) have important technological significance for many applications including optical communications and optical signal processing. They can function as differential amplifiers, switches, limiters, clippers and regenerative oscillators. Several different realizations of bistable optical devices have been demonstrated recently[1-4]. These fall into two broad classes: the all-optical devices and the hybrid variety which combines optical and electronic elements. In both cases the steady state properties have been studied extensively. Relatively little work, however, has been done on their transient behaviour. In this letter, we report the results of a detailed study of the dynamics of a hybrid bistable optical device. The experimental results confirm theoretical predictions concerning the dependence of switching time on the applied light increment. For the first time, the phenomenon of "critical slowing down" which limits the switching speed is observed directly.

The lengthening of switching time near the critical input intensity was predicted theoretically by Bonifacio and Lugiato[5] in an analysis of two-level atoms within a Fabry-Perot resonator. In another time-dependent study, McCall[6] discussed

the possibility of regenerative oscillations in a BOD. Recently Bischofberger and Shen[7] studied the transient behaviour of a Fabry-Perot resonator filled with a Kerr medium. They measured transmitted pulse distortion to infer the transient properties of the system. In our experiments, we investigate the response of a hybrid BOD to step inputs of light using a 0.5 mW cw HeNe laser. The time constants of our system are determined electronically and can be varied easily.

Figure 1a shows the experimental configuration drawn to emphasize the functional similarity between electrical and optical signals. It consists of a Pockels cell modulator M driven by the output of a photoconductor PC and is described in detail in Ref. 3. For these transient response studies, a capacitor C has been added across the load resistor. Fig. 1b shows the steady state transfer curve (intensity out vs. intensity in) with axes labelled in voltage units. This transfer curve was measured for a modulator whose transmission T(V) was that shown in the inset and could be described approximately by

$$T(V) = \tfrac{1}{2}\left| 1 - 0.6 \cos \{\pi(V + 40)/220\} \right| . \qquad (1)$$

On the transfer curve in Fig. 1b are shown V_{ac} and V_{oc}, the

critical input for switching and the critical output just before switching. The aim of this paper is to study the transient response versus the switching increment $\nu \equiv (V_{in} - V_{ac})/V_{ac}$, where V_{in} is the incident intensity in voltage units. The arrows on the transfer curve indicate the values of V_{in} actually used in the experiment.

The transient response of bistable optical devices is governed by two sources of delay: 1) response time τ_1 of the output voltage to changes in input signal, and 2) response time τ_2 of the control voltage to changes in output voltage. In an all-optical device employing a Fabry-Perot interferometer, τ_1 includes cavity buildup time and τ_2 includes the response time of the nonlinear index. In our mirrorless hybrid device, τ_1 is the response time of the detector current, and τ_2 is that of the circuitry driving the Pockels voltage. Using a simple relaxation equation for each contribution leads to the general equation

$$\tau_1 \tau_2 V'' + (\tau_1 + \tau_2) V' = V_{in} T (V + V_B) - V \qquad (2)$$

for the variable part of the control voltage (primes are time derivatives). We emphasize that this form is an approximate model for all types of nonresonant bistable devices. It gives the qualitative features observed in the experiments of Bischofberger and Shen[7], and admits analytical estimates

of device behavior. Furthermore, it can be shown that this equation describes exactly the hybrid electrical - optical circuit shown in Fig. 1a.

In our experiments, the time constant τ_2 is essentially that of the detector load, and was chosen to be 0.2 sec. The detector rise time was $\tau_1 \simeq 10^{-2}$ sec. The incident intensity was suddenly stepped to a value given by V_{in}, and the output intensity was observed on a chart recorder as a function of time. Fig. 2a shows I_{out} vs. time for three values of switching increment . Notice the overshoots for large ν, and the nonlinear slowing down for small ν. Theoretical curves obtained from Eqs (1) and (2) with experimental values of the parameters are shown in Fig. 2b. Agreement is good to within experimental error.

The BOD response time τ, defined as the time required for the output to reach 1/e of the steady state value, is a decreasing function of ν. In Fig. 3 are shown the experimentally determined values of τ vs. ν. The theoretical curve in this figure was obtained from Eq. (2) by ignoring the first term, an approximation which is excellent when considering the slow change of the system as it turns on past the "nose" at (V_{ac}, V_{oc}) in Fig. 1b. The resulting first order equation can be integrated approximately by

replacing the right side of Eq. (2) by a polynomial P(V). Then the integral of 1/P(V) passes near a pole in the complex V plane corresponding to the nose in Fig. 1b. For switching increments small relative to the distance to the next nose, only this pole need be kept to describe accurately the nose region. Keeping also the pole corresponding to the switched-on steady state, one may integrate to find the effective response time

$$\tau/\tau_2 \simeq (1-V_{in}T')^{-1} + 2\pi\,\nu^{-\frac{1}{2}}\{A\,(1+\nu)\,-\nu\}^{-\frac{1}{2}} \qquad (3)$$

where $A = 2T_o''\,V_{oc}\,V_{ac}$, $T_o'' = T''(V_{oc})$, and T' is evaluated at the switched-on steady state. Exact numerical integration of Eq. (2) indicates that Eq. (3) is accurate to within 10% for our parameters. Furthermore, for the switching intensities of interest, the first term in Eq. (3) represents a linear response time which is much smaller than the second term and hence can be neglected.

Eq. (3) and Fig. 3 indicate that the response time diverges for small ν. This is the "critical slowing down" phenomenon. As the switching increment increases, the response time approaches that of the circuit time constant.

The energy in a pulse required to switch the BOD is proportional to the product of the switching intensity and the effective switching time τ. From Eq. (3), we find that the switching energy is

$$E = V_{in}\,\tau = 2\pi\nu^{-\frac{1}{2}}\{A(1+\nu) - \nu\}^{-\frac{1}{2}}\,V_{in}\,\tau_2. \qquad (4)$$

Equation (4) shows that the switching energy tends to infinity as $\nu \to 0$, i.e. near the minimum intensity required for switching. As the switching level decreases to less than twice the minimum switching intensity ($\nu < 1$), not only does the switching time increase (critical slowing down), but the switching energy increases. This means that the energy which is estimated from steady state considerations, as done for example in Ref. 8, is not accurate at these switching levels.

For $V_{in} > 2V_{ac}$, the switching energy decreases rapidly to an asymptotic value,

$$E = 2\pi\,(A - 1)^{-\frac{1}{2}}\,V_{ac}\,\tau_2 \qquad (5)$$

Clearly the switching energy can be minimized by increasing A.

In order to obtain a physical picture for A, consider the case of a sinusoidal modulator, where

$$T(V) = \tfrac{1}{2}\{1 - F\cos\,(V + V_B)\}\ .$$

In this case

$$A = 2\,V_{oc}\,\mathrm{Tan}^{-1}(V_{oc} + V_B) \qquad (6)$$

It can be shown that this quantity is a rapidly increasing

function of the extinction factor F. Thus, to minimize the switching energy, it is necessary to use devices with high extinction ratios. In practice, however, large values of F have the disadvantage of requiring high switching intensities. For any given application, there will be an optimum value of F, and Eq. (5) will give the switching energy for this value.

In conclusion, we have studied the transient behaviour of a hybrid BOD and confirmed the critical slowing down which limits the response time and increases the switching energy at low input intensities. Higher input intensities ensure faster response times and lower switching energies.

The authors gratefully acknowledge Albert Chen for assistance with the experiments. This work was sponsored in part by RADC, Hanscom Air Force Base, Mass. and in part by AFOSR.

REFERENCES

1. H.M. Gibbs, S.L. McCall, T.N.C. Venkatesan, Phys. Rev. Lett. 36, 1135 (1976).
2. P.W. Smith, E.H. Turner, Appl. Phys. Lett. 30, 280 (1977).
3. E. Garmire, J.H. Marburger, S.D. Allen, Appl. Phys. Lett. 32, 320 (1978)

   J. Marburger, S.D. Allen, E. Garmire, M. Levenson, H. Winful, International Quantum Electronics Conference X, Atlanta, Ga., May 1978). Digest of Technical Papers, p. 642.
4. A Feldman, Appl. Phys. Lett. 33, 243, (1978).
5. R. Bonifacio, A.L. Lugiato, Opt. Comm. 19, 172, 1976.
6. S.L. McCall, Appl. Phys. Lett. 32, 284 (1978).
7. T. Bischofberger, Y.R. Shen, Appl. Phys. Lett. 32, 156 (1978)

FIGURE CAPTIONS

Fig. 1 (a) Simplified schematic of a hybrid bistable optical device. M = modulator, PC = photoconductor, V_B = bias voltage.

(b) Measured steady state transfer curve using modulator whose transmission as a function of voltage is shown in the inset.

Fig. 2 (a) Experimental curves showing BOD output as a function of time for three different step inputs. The values of the incremental switching intensity are A) $\nu = 4.6$ B) $\nu = 1.4$ C) $\nu = .03$

(b) Theoretical curves of output signal vs. time, generated by solving Eq. (2) with incremental switching intensities of

A) $\nu = 4.6$ B) $\nu = 1.0$ C) $\nu = .01$

Fig. 3 Characteristic switching time versus increment of input switching signal beyond critical value. The theoretical plot was obtained from Eq. (2).

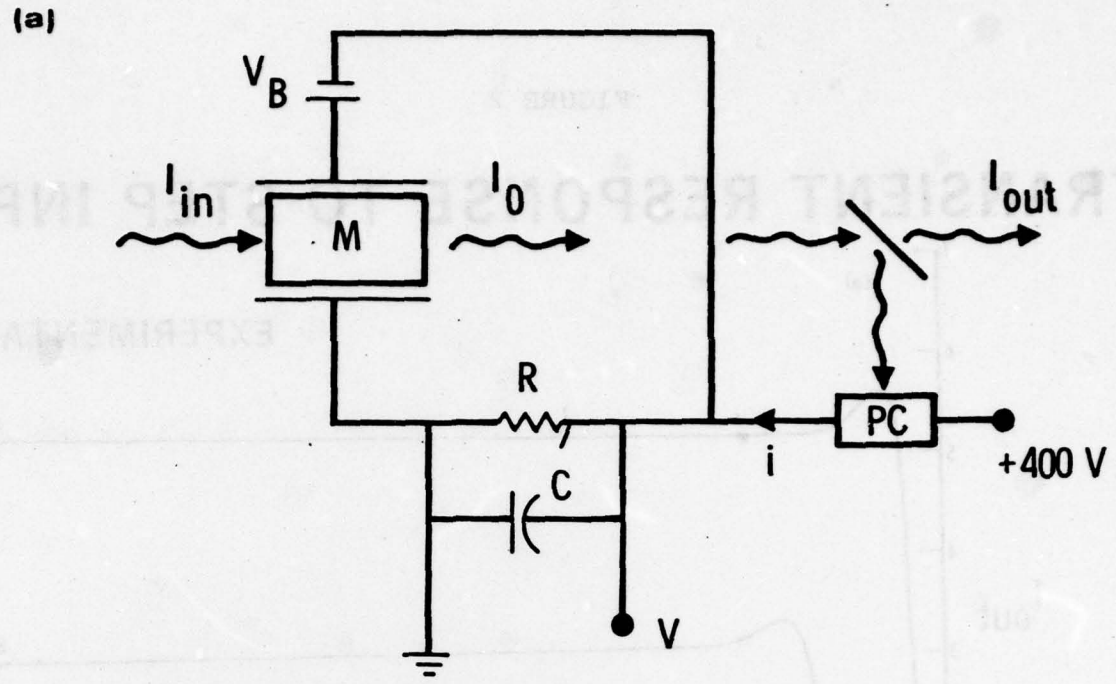

Figure 1-a. Simplified schematic of a hybrid bistable optical device. M = modulator, PC = photoconductor, V_B = bias voltage.

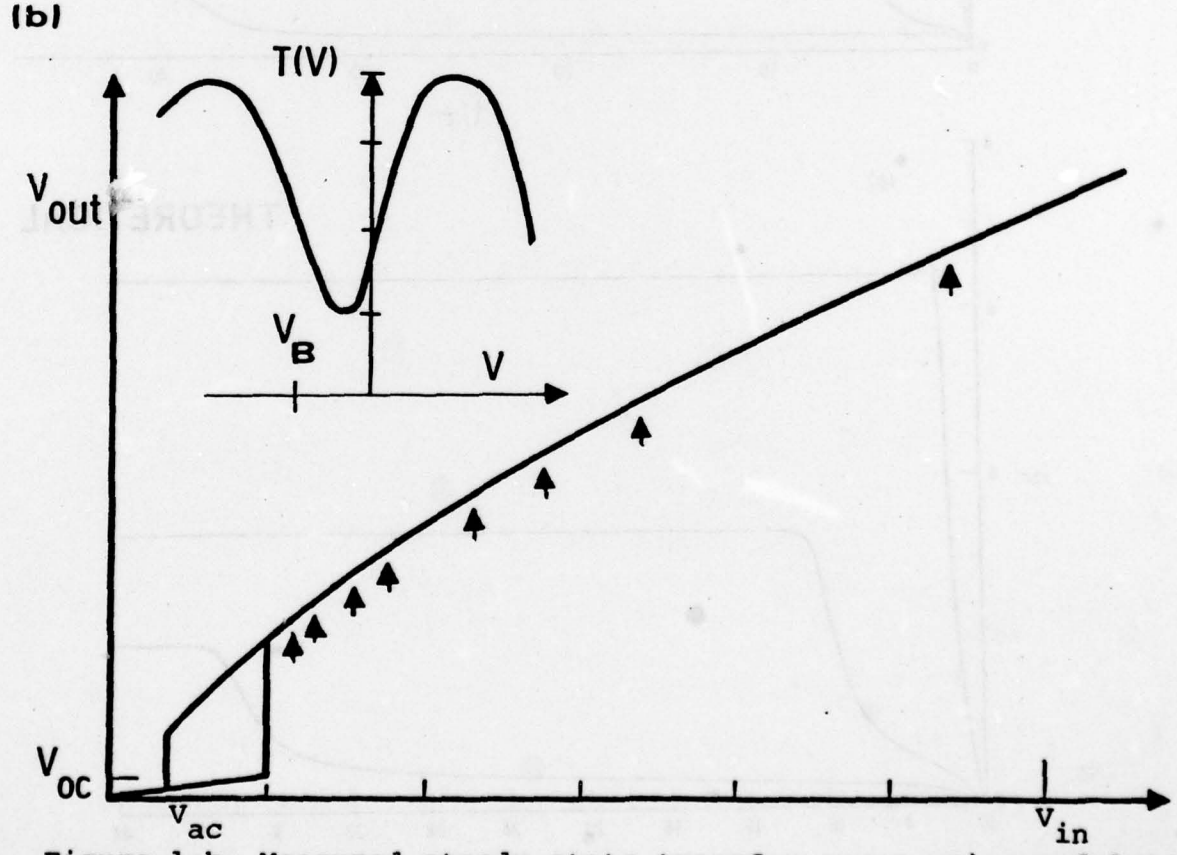

Figure 1-b. Measured steady state transfer curve using modulator whose transmission as a function of voltage is shown in the insert

FIGURE 2

TRANSIENT RESPONSE TO STEP INPUT

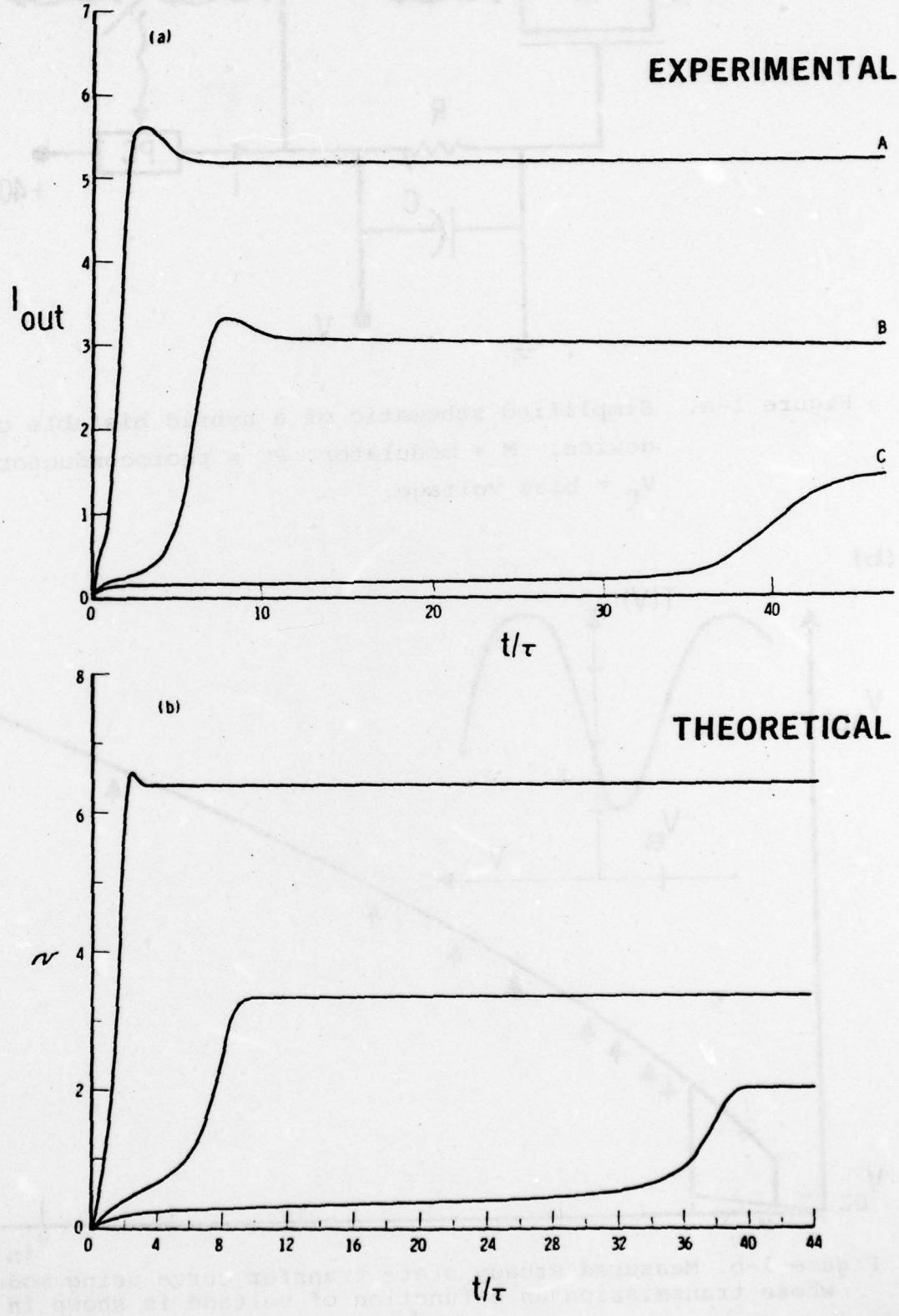

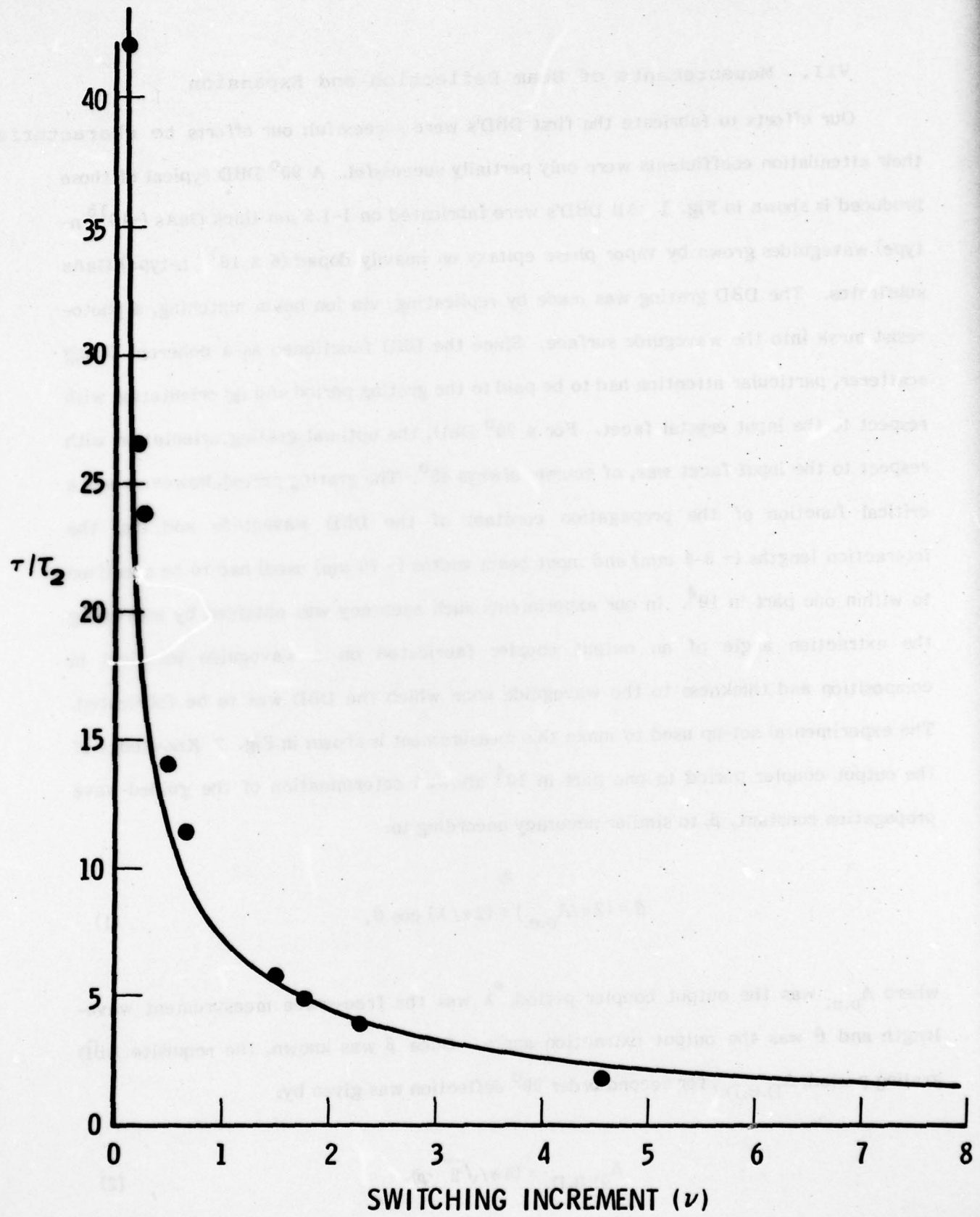

Figure 3. Characteristic switching time versus increment of input switching signal beyond critical value. The theoretical plot was obtained from Eq. (2).

VII. Measurements of Beam Deflection and Expansion

Our efforts to fabricate the first DBD's were successful; our efforts to characterize their attenuation coefficients were only partially successful. A 90^{o} DBD typical of those produced is shown in Fig. 1 All DBD's were fabricated on 1-1.5 μm thick GaAs (~10^{15} n-type) waveguides grown by vapor phase epitaxy on heavily doped (6×10^{18} n-type) GaAs substrates. The DBD grating was made by replicating, via ion beam matching, a photoresist mask into the waveguide surface. Since the DBD functioned as a coherent Bragg scatterer, particular attention had to be paid to the grating period and its orientation with respect to the input crystal facet. For a 90^{o} DBD, the optimal grating orientation with respect to the input facet was, of course, always 45^{o}. The grating period, however. was a critical function of the propagation constant of the DBD waveguide and (for the interaction lengths (~ 3-4 mm) and input beam widths (~ 70 μm) used) had to be specified to within one part in 10^{4}. In our experiments such accuracy was obtained by measuring the extraction angle of an output coupler fabricated on a waveguide identical in composition and thickness to the waveguide upon which the DBD was to be fabricated. The experimental set-up used to make this measurement is shown in Fig. 2 Knowledge of the output coupler period to one part in 10^{4} allowed determination of the guided-wave propagation constant, β, to similar accuracy according to:

$$\beta = (2\pi/\Lambda_{o.c.}) + (2\pi/\lambda)\cos\theta, \tag{1}$$

where $\Lambda_{o.c.}$ was the output coupler period, λ was the free-space measurement wavelength and θ was the output extraction angle. Once β was known, the requisite DBD grating period, $\Lambda_{D.B.D.}$, for second order 90^{o} deflection was given by:

$$\Lambda_{D.B.D.} = (4\pi/\sqrt{2}\cdot\beta). \tag{2}$$

It was our intention to infer a given DBD attenuation coefficient by examining a semi-logarithmic plot of the deflected beam, near-field pattern. Our attempts to follow this procedure, however, were frustrated by the inherent weakness of the deflection process for the type of GaAs on n^+-GaAs waveguides used. The free-carrier, plasma depression effect responsible for the guide/substrate index discontinuity was simply not great enough to simulate, adequately, the large refractive index discontinuities available with the GaA1As waveguides which would ultimately be used. Partial solution to this problem (pending growth of suitable GaA1As waveguides) was obtained by noting that the DBD attenuation coefficient varied as $(n_2^2 - n_1^2)^2$ where n_1 was the real part of the superstrate refractive index (normally equal to 1 for air) and n_2 was the waveguide refractive index. By choosing a metallic superstrate such as aluminum, therefore, for which $n_1^2 = -69$, a substantial increase in DBD deflection efficiency was expected and, indeed, observed.

Figures 3a and 3b show linear and semi-logarithmic plots of a deflected beam, near-field pattern obtained from an aluminum coated DBD. Ideally, the semi-logarithmic plot should have been a straight line whose slope equaled the DBD attenuation coefficient. Unfortunately, however, the aluminum overlayer, through its imaginary refractive index component, led to mode conversion and ohmic loss effects, which prevented observation of the desired phenomena. While accurate measurement of the DBD attenuation coefficients could not, therefore, be obtained from these devices, data relating deflection efficiency to input beam angle-of-incidence was obtained. This data, shown in Fig. 4, was used to corroborate theoretical estimates of angular sensitivity and grating period/orientation tolerances.

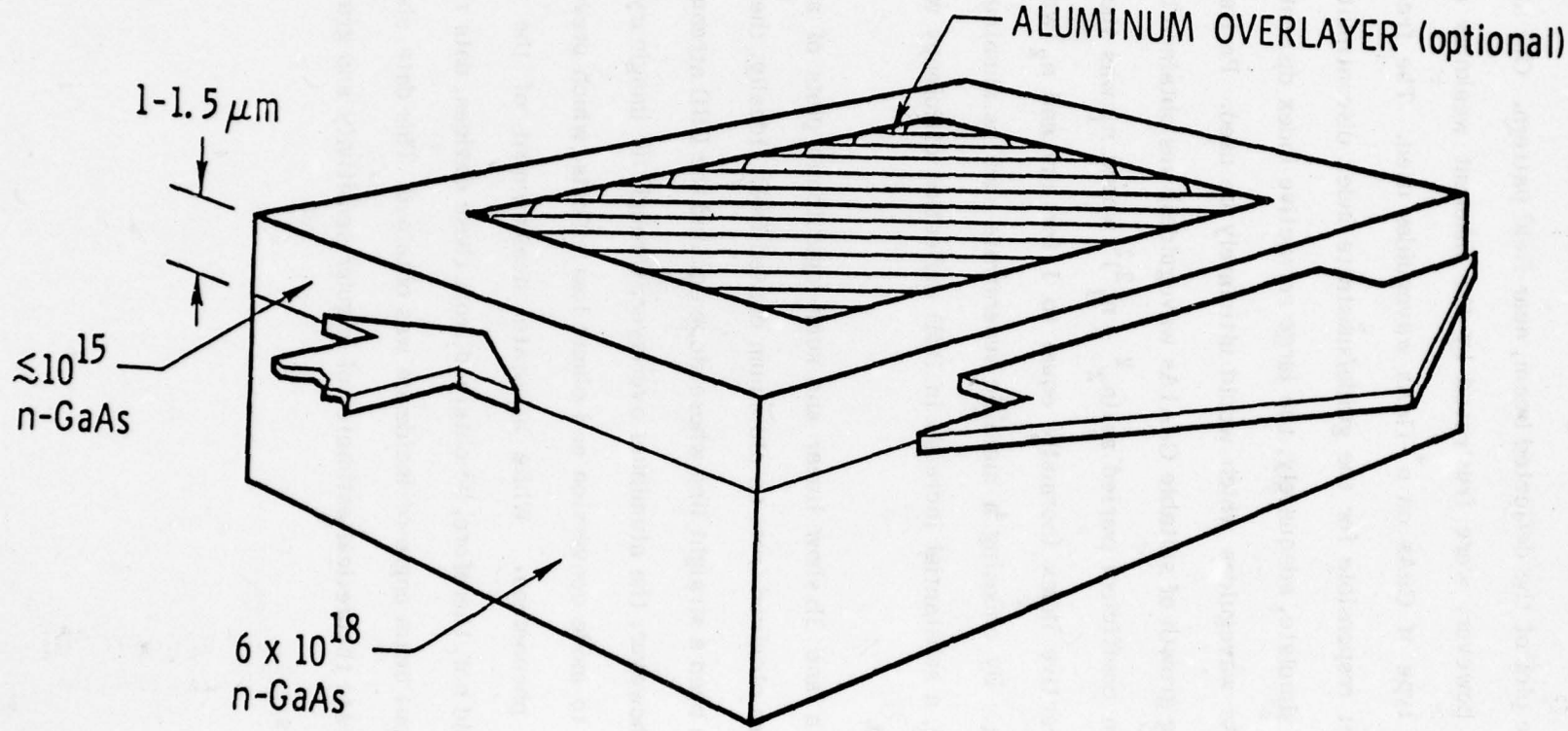

Fig. 1 Perspective of typical DBD fabricated.

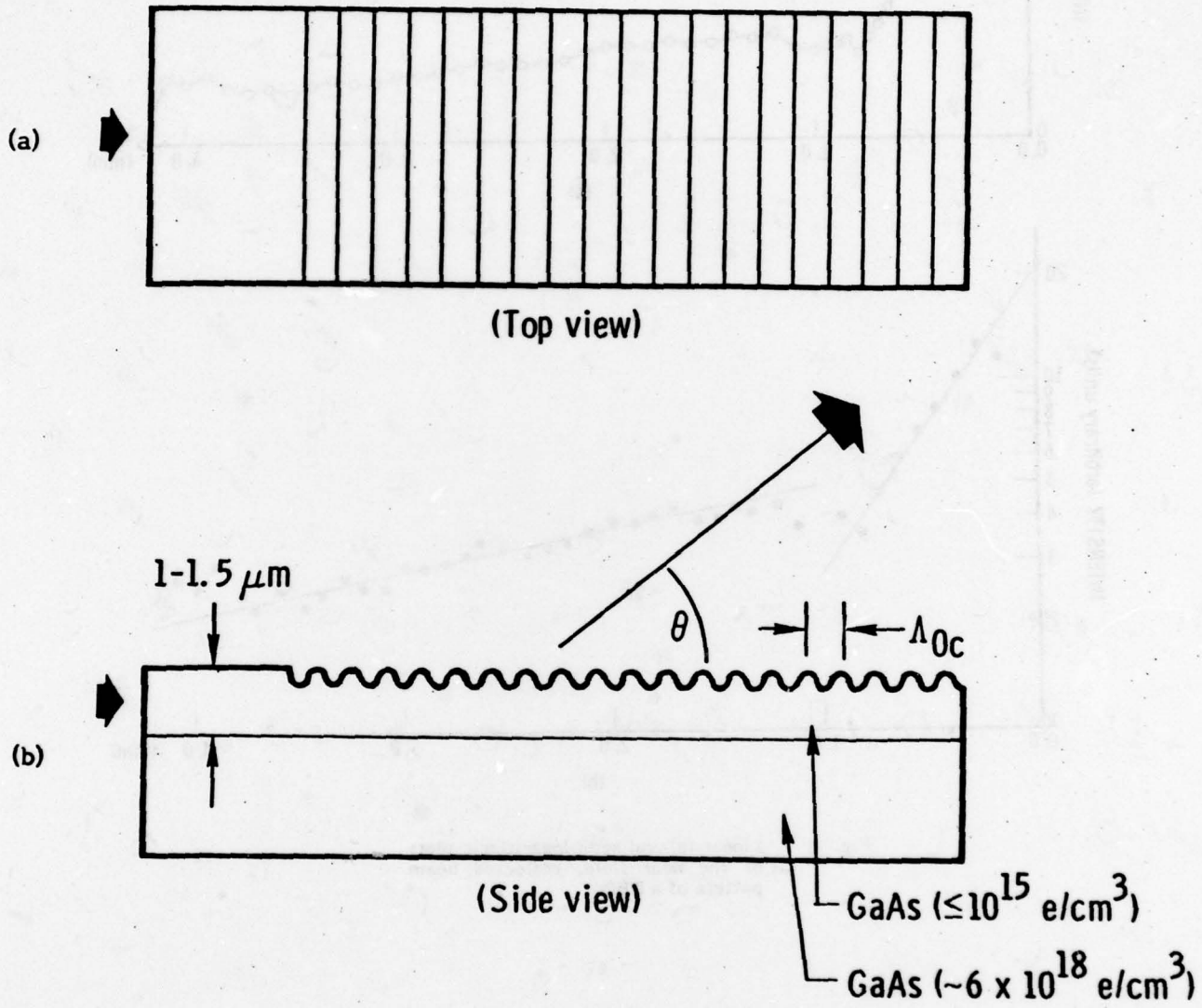

Fig. 2 Top (a) and cross sectional (b) views of output grating coupler used to measure waveguide propagation constant, β.

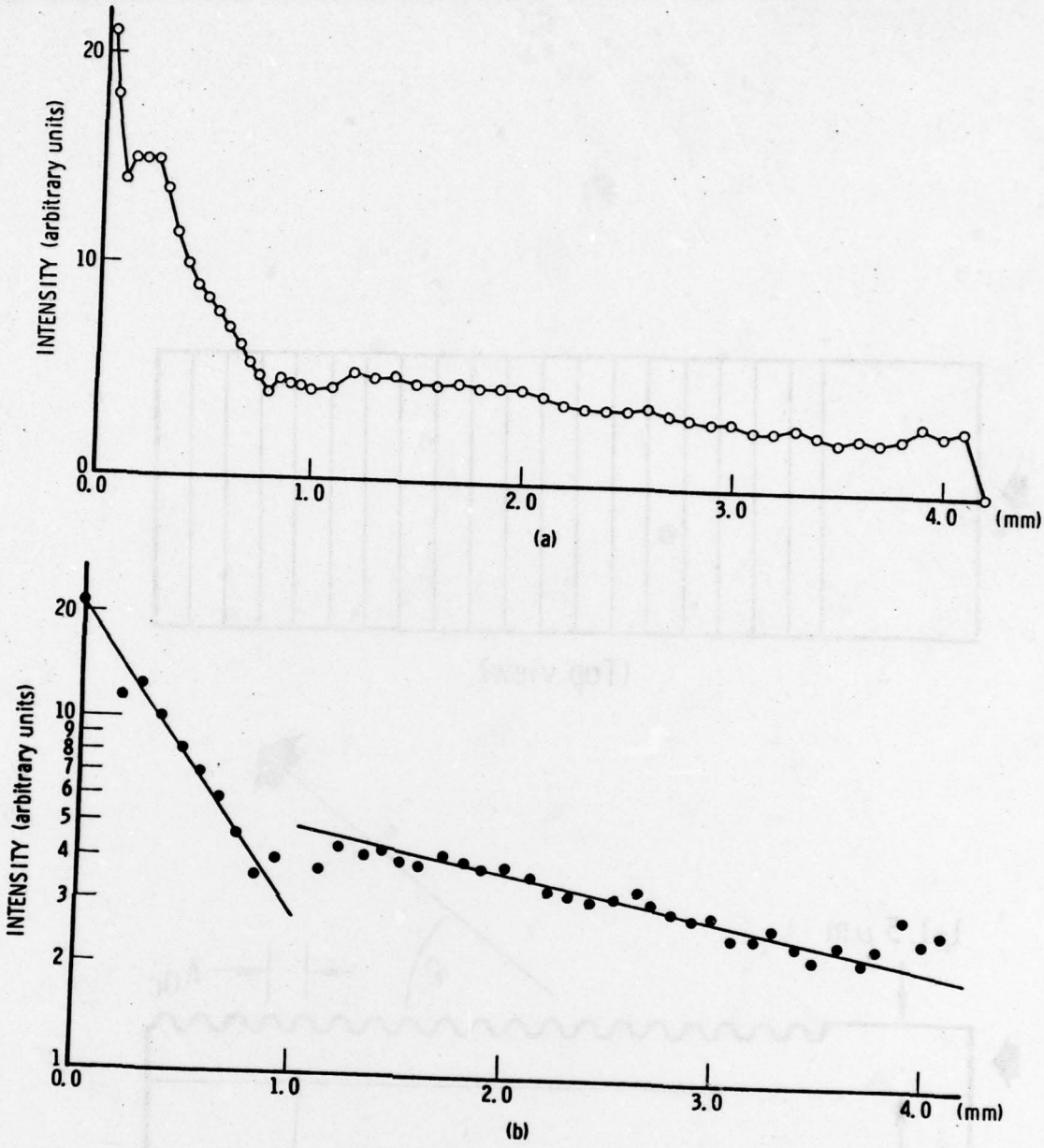

Fig. 3 Linear (a) and semi-logarithmic plots of the near field, deflected beam pattern of a DBD.

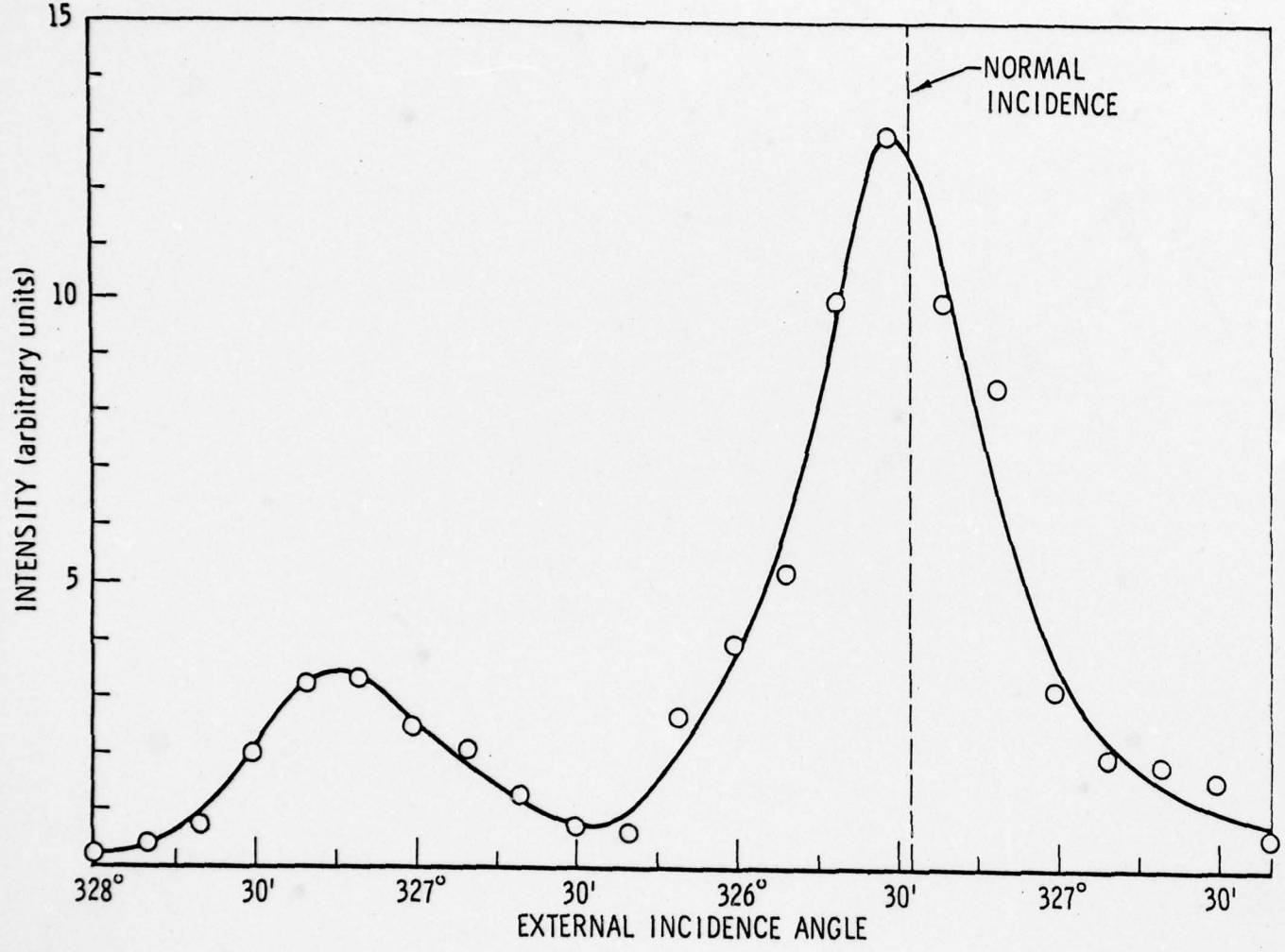

Fig. 4 DBD, deflected beam intensity as a function of input beam angle-of-incidence within the plane of the wave guide.

MISSION
of
Rome Air Development Center

RADC plans and executes research, development, test and selected acquisition programs in support of Command, Control Communications and Intelligence (C^3I) activities. Technical and engineering support within areas of technical competence is provided to ESD Program Offices (POs) and other ESD elements. The principal technical mission areas are communications, electromagnetic guidance and control, surveillance of ground and aerospace objects, intelligence data collection and handling, information system technology, ionospheric propagation, solid state sciences, microwave physics and electronic reliability, maintainability and compatibility.

Printed by
United States Air Force
Hanscom AFB, Mass. 01731